

SLAC-PUB-16137

Conceptual Design for the New RPI 2020 Linac

RPI 2020 Linac Design Study Group

October 29, 2014

Prepared for BMPC-KAPL under purchase order number 103313
by SLAC National Accelerator Laboratory.

RPI 2020 Linac Design Study Group

C. Adolphsen, K. Bane, V. Dolgashev, A. Jensen, A. Haase, E. Jongewaard, M. Kemp, A. Krasnykh, J. Lewandowski, Z. Li, J. Neilson, C. Pearson, S. Tantawi, J. Wang, A.D. Yeremian: SLAC National Accelerator Laboratory, Menlo Park, California

P. Brand, Y. Danon, Rensselaer Polytechnic Institute, Troy, New York

B. Epping, T. Donovan, R. Block, G. Leinweber, BMPC-KAPL, Troy, New York

Acknowledgments:

The conceptual design for the RPI 2020 L-band Linac relies heavily on the experience of the people who designed, commissioned and operate several linear accelerators at SLAC, the longest of which is the SLAC 2-mile S-band linac. In addition the conceptual design owes much to the close cooperation with scientists and engineers at Rensselaer Polytechnic Institute (RPI) and Bechtel Marine Propulsion Corporation – Knolls Atomic Power Laboratory (BMPC-KAPL), who have formulated the goals of the future machine and provided the necessary detailed information about existing infrastructure and capability at RPI. Finally the RPI 2020 Linac Design Study Group is a list of people, authors and non-authors, who have contributed significantly to this conceptual design.

In the process of completing this conceptual design for the RPI 2020 Linac, we have held one kickoff meeting at RPI, several phone meetings with RPI and BMPC-KAPL, an internal review at SLAC, presented an interim draft to RPI and BMC-KAPL half way through the process, incorporated BMPC-KAPL and RPI returned comments into the draft report, presented a final draft to BMPC-KAPL and RPI, held a close-out meeting with BMPC-KAPL and RPI at SLAC, and incorporated BMPC-KAPL and RPI returned comments into the final report. We thank everyone who has made it possible to create the conceptual design for the RPI 2020 linac and this report.

Table of Contents:

Introduction	1
Electron Beam Specifications and Linac Requirements	4
Short Pulse Operation	4
Low Rep Rate Operation.....	5
High Power Operation	5
Low Energy (10 to 20 MeV) Operation	6
Conceptual Design for New RPI 2020 Linac	8
Injector.....	10
Electron Gun.....	13
Bunching System	15
Injector Magnetic System.....	17
Injector Apertures and Diagnostics	17
Injector Power Sources.....	19
Speed-of-Light Accelerator System	19
Accelerator Structures.....	19
RF Sources	23
Modulators.....	24
Magnetic Focusing and Steering.....	27
Diagnostics	28
Vacuum, Temperature Stabilization, Machine Protection	28
Proposed Multiphase Program for RPI Machine Development	30
Phase 1: Conceptual Design	30
Phase 2: Linac Design: Program Plan and Cost Estimate	30
Phase 3: Construction Phase.....	31
Phase 4: Commissioning Phase	32
Summary.....	33
Appendix A: Alternative Accelerator Designs.....	34
Appendix B: Bunch stacker	39
Appendix C: RF Pulse Compression	42
Appendix D : SLAC Surplus.....	43
References	44

Introduction

The Rensselaer Polytechnic Institute (RPI) spectrometer is an installation based on an L-band linear accelerator designed and installed many decades ago. While this installation has served many important experiments over the decades, a new more powerful and more flexible linac to serve a wider range of experiments is envisioned as an upgrade to the existing installation by 2020. The three main priority experiments for the new RPI 2020 L-band linac can be categorized as follows:

- 1) The first and highest priority is the neutron production experiments to support current and future nuclear cross-section work by both Bechtel Marine Propulsion Corporation – Knolls Atomic Power Laboratory (BMPC-KAPL) and the Nuclear Criticality and Safety Program (NCSP). These experiments aim to enhance the nuclear data bank libraries that are critical for designing efficient nuclear reactors as fossil-fuel alternatives for energy. These include keV to MeV neutron cross-section measurements and thermal cross section measurements. These experiments require short pulse-widths (5.4 to 250 ns), up to 150 MeV electron beams, and pulse repetition rates from 25 to 800 Hz.
- 2) The second priority experiments at RPI are for isotope production research and development as well as electronic/detector testing. Isotopes have many practical and beneficial applications ranging from nuclear medicine to electronics testing. These experiments require several tens of kW average electron beam power from electron pulses within the volume where the isotopes are generated. At RPI the electron beam requirements are up to 150 MeV, on the order of microseconds pulse width and pulse repetition rates from 1Hz to as high as possible.
- 3) A third priority for the RPI L-band linac is supporting a collection of non-nuclear experiments whose purpose ranges from material modification to electronics testing. A low energy configuration is necessary to meet the operational needs of this set of experiments.

The current RPI L-band electron linac is limited to approximately 60 MeV electron beam energy and 10 kW average electron beam power. Ideally electron energies of up to 150 MeV and average electron beam powers from 1 kW to several tens of kW are needed for the complete range of experiments envisioned at RPI.

The high priority pulsed neutron source experiment at RPI is based on a photo-neutron (γ, n) reaction. The electrons accelerated in the linac and incident on the target/converter are decelerated to produce a wide spectrum of X-ray flux. This photon flux intensity and spectrum are sufficient to evaporate neutrons from atoms and generate a neutron pulse. The number of generated neutrons is proportional to the number of incident electrons. However the neutron yield with respect to electron energy has dual slopes separated by a “knee” for heavy target materials. Figure 1 shows the neutron yield curves for various target materials [1]. As can be seen in Figure 1, the neutron yield slope is linear, steep, and positive from ~ 10 to 20 MeV and linear, gentle, and positive in the region ≥ 50 MeV. The knee is between 20 and 50 MeV, and neutron production is sharply cut off at < 10 MeV.

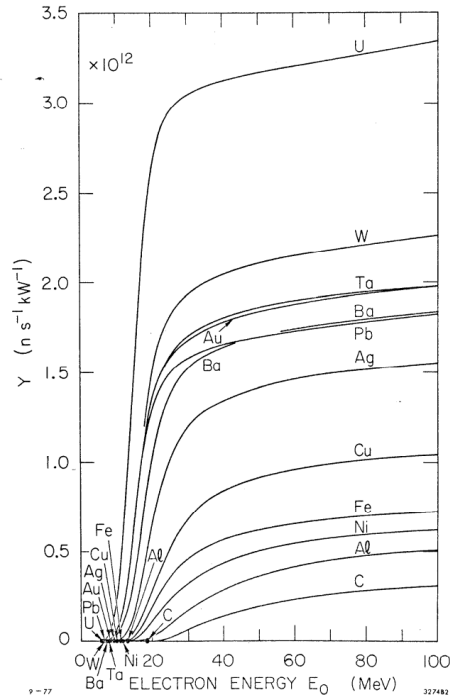


Figure 1. Neutron yield curves for various target materials

The diagram shows that there are no resonances, thus on the plateau there is practically no restriction on the electron energy spread. Hence at electron energies >50 MeV the neutron yield is directly proportional to the average beam power and practically independent of the beam energy. At RPI, electron energies between 60 and 150 MeV are desired for the highest yield limited by the shielding considerations in the current RPI accelerator hall.

Traditional neutron sources are based on either ion (protons or other) accelerators (cyclotrons, synchrotrons, or linacs) to produce a beam to bombard on a converter target or nuclear reactors that can directly produce neutrons. The ion accelerators are inefficient devices for neutron production because ion energies incident on the converter target need to be >1 GeV to generate neutrons via a spallation process. Reactor-based pulsed neutron sources are inefficient and expensive and generate nuclear waste, which is very difficult to dispose of. Additionally there is a need for extensive nuclear safety restrictions and regulations on the operation of such reactors. The cost of both ion based and reactor based neutron production is at least an order of magnitude greater than the upgraded electron linac envisioned for RPI by 2020.

An additional advantage of neutron production by high-energy electrons is that they penetrate deep into the converter target and their energy deposition in a volume is much more uniform compared to protons and other ions. This feature simplifies the converter target cooling for neutron production with electron sources compared to ion sources.

The existing RPI infrastructure is very well suited to support the most efficient, effective, and inexpensive option of upgrading the L-band linac in the existing hall to more than double the currently achievable energy and average power of the electron beam.

The current RPI linac accelerator sections were designed some fifty years ago based on linac technology and tools available at the time. Since then many new techniques for designing, building, and operating linear accelerators have been developed. These techniques will be applied to the new RPI machine in order for it to meet the very wide range of operating parameters required for the large range of experiments envisioned on the new RPI 2020 accelerator. With sixty years of experience in designing, constructing, commissioning, and operating multiple high-energy linacs, SLAC National Accelerator Laboratory has demonstrated the capabilities to provide RPI the design expertise to achieve their operational goals for the new linac.

Electron Beam Specifications and Linac Requirements

Based on the specifications received from RPI [2], the new RPI 2020 accelerator needs to meet four basic modes of operation in order to serve all the users envisioned. The operational modes and allowable range of beam parameters are listed in order of priority in Table 1. Meeting the requirements of the operating modes requires wide range of operating parameters of the linac. Each of the modes of operation has its particular challenges, which, combined with the power available from the klystrons and modulators, define the basic footprint of the linac.

Table 1. The four basic operation modes that the new RPI 2020 electron linac must accommodate listed in order of priority

Operation mode	Pulse Width (ns)	Rep. Rate (Hz)	Beam Energy (MeV)	Pulse Current (A)	Average Beam Power (kW)
Short Pulse	<6	≤800	60 – 150	As needed	≥7
Low Rep. Rate.	<250	25	60 - 150	As needed	≥1
High Power	Any	≤800	45 - 150	As needed	≤45
Low Energy	0 to ≥ 25	single to Maximum	10 - 20	0-10	any

Short Pulse Operation

Short pulse operation has been identified by RPI as the most important operational parameter, requiring an average beam power ≥ 7 kW with a < 6 ns pulse width. The key issues that require special attention in the linac design for short pulse operation are:

- a) Achieving high current (≥ 18 A in the pulse) from the gun and 11 to 14 A at the exit of the accelerator. We believe the existing RPI gun with a 3 cm^2 cathode, possibly with some modification of the A-K region, should be able to achieve this current. However this must be verified with beam simulations and experimentally proven.
- b) Evaluation of wakefield effects on the beam dynamics from high single bunch current (130 to 300 amps) operation is of importance. The primary method to mitigate wakefield effects is by increasing the aperture diameter of the accelerator. However using these techniques requires increases in the rf drive power to maintain the same beam energy. To help compensate for this problem, nose cones on the aperture irises can be added to increase the shunt impedance though at the expense of increasing construction complexity/cost. Thus consideration of the most

efficient use of the rf power possible, while also mitigating wakefield effects, must be part of the design scenario to achieve the short-pulse, high-peak-current electron beam parameters.

Low Rep Rate Operation

To achieve the ≥ 1 kW average electron beam power with only 25 Hz pulse repetition rate and < 250 ns pulse length, about 1.5 A pulse current is required at 130 to 150 MeV operation. The primary concern here is the beam break up (BBU), where the fields induced on the accelerator walls by the previous bunches act on the bunches that arrive later in the pulse train. This phenomenon sets the peak allowable current and pulse width. In the short-pulse (< 6 ns) mode of operation, the train is likely not long enough to be disrupted by BBU, but in the 250 ns case this issue must be taken into consideration, though it is not as severe as in the next case of pulses in the μ sec range. Mitigation of BBU calls for increasing apertures as large as possible and variation of the cell geometry along the structure. Mitigation of potential BBU must also be balanced against the increased rf power requirements and construction complexity.

High Power Operation

In this mode of operation the challenges are beam loading compensation, BBU and the high average power of ≤ 45 kW. As the electron pulse travels through the accelerating structure, it imparts its own energy to the structure while it also gains energy from the rf energy stored in the structure. The amount of energy that the electron can impart back to the structure does not depend on whether or not the structure is filled with rf. It does depend on the electron beam current in the pulse. In a Traveling Wave (TW) structure, if the electron pulse is injected after the structure is filled, the energy of the front portion of the electron pulse will drop at an exponential rate for the duration of the structure fill time and then remain at steady state as the beam continues to impart its energy back to the structure at the same rate as the structure continues to fill with rf. Thus the stored energy in the structure must be greater than the energy that the beam imparts back to the structure in order for the whole beam pulse to gain energy. To mitigate the front portion of the energy variation from the bunch that occurs at one fill time and beyond into the electron beam pulse length, an early injection method of compensation is employed in traveling wave structures. In this case, the front portion of the electron beam pulse arrives while the structure is not yet completely filled, and it reaches the end of the structure at a time when it cannot gain as much energy there as the bunches that arrive later when the structure is more filled. One filling time later, when the accelerator has been completely filled, a steady state occurs. In this way the beam energy variation in the transient portion of the pulse (the front portion of the pulse that is one filling time or less long) can be minimized; the concept is called “transient beam loading compensation” in TW accelerators. While the energy drop in the electron beam pulse is not of much consequence to RPI’s experimenters, managing it to about $\pm 5\%$ level is important from the magnetic optics point of view to contain the beam in the transverse direction. Thus for the high-power, long-pulse mode of operation, having sufficient peak rf power to compensate the pulse beam loading energy and enough average rf power to achieve the high average beam power requirements are the key issues. That means the klystron and modulator must have sufficient peak and average power and pulse length to accommodate the long pulse beam and its beam loading compensation. Other high-power operation

considerations include automated machine protection controls to shut off the beam or reduce it to a much lower average power mode when the beam behavior is altered from optimal due to a component failure or human error of inserting a diagnostic device while the beam is on at high power. Sufficient automated machine protection controls are necessary to ensure successful and reliable operation.

Low Energy (10 to 20 MeV) Operation

In this mode of operation, the key issues are (1) being able to achieve and transport energies as low as 10 to 20 MeV while compensating the transient beam energy variation down to an acceptable level and (2) mitigating wakefield effects throughout the entire machine when such a low energy beam needs to travel through many structures. This involves the following considerations:

a) In order to achieve beam energies as low as 10 MeV, the beam from the injector beam line must be < 10 MeV, as the accelerator sections should only add energy to the beam and the final energy of the beam cannot be lower than the beam energy out of the injector. Since the injector design scenario is dominated by space charge and bunching considerations, the beam energy out of the injector will be chosen so as to minimize the bunch length and achieve manageable space charge forces as it travels to the following accelerator section while at the same time keeping the beam energy at < 10 MeV. Once the beam is bunched to its minimum bunch length and reaches nearly the speed of light, the remainder of energy gain is best achieved in the accelerator sections. Since the electrons travel at 99% of the speed of light by the time they reach 5 MeV, the beam energy out of the injector should be approximately 5 MeV for all scenarios and the remainder of the acceleration should be accomplished in the subsequent accelerator sections. On the other hand, at low energy and high bunch currents, the space charge forces can have dominant effect pushing the beam outwards in both the transverse and longitudinal directions. Thus the drift distance between the injector and first accelerator section cannot be too long. Since the best machine scenario is one where the injector parameters are left the same from operating mode to operating mode, the lowest energy operation pretty much defines the upper-most limit of the energy from the injector.

b) Another important consideration for this mode of operation is the transport systems. As mentioned above, when the beam travels through the accelerator sections, it loses its energy to the structure, and it does not matter whether or not the structure is filled with accelerating rf. Thus the klystrons need to provide only a little bit of power to accelerate the beam beyond 5 MeV, plus sufficient power to compensate for the beam's own energy loading compensation. It basically means that the accelerator must impart only about 5 to 15 MeV more energy to the beam and do it in a transient beam loading compensated manner. However for high current cases (~ 10 A), the energy that the beam would deliver on all the structures combined can be as high as 20 MeV by the time it gets to the end of the entire linac. This means that if we fill the structure such that we accelerate the first bunch up to 20 MeV, the last bunch will have no energy at all. In order to achieve a mean energy of 20 MeV, the front bunch would have to be accelerated to 30 MeV and the final bunch to 10 MeV in the very short pulse case (25 ns), where the beam loading is somewhat linear. This very low energy and very large energy spread beam

then needs to be transported through the entire length of the machine to the experiment with quadrupole focusing, which will not have such a wide energy spread acceptance. This very low energy and very large energy spread beam would play havoc on the beam transport system.

c) And finally, an important consideration is that at about 10 - 20 MeV, the beam is not as “stiff” as at the higher 60 – 150 MeV energies and all adverse effects such as external magnetic fields from pumps and current carrying conductors for the magnets, BBU and even space charge to some extent, all have an enhanced effect on the beam at these low energies, making it difficult to transport it for long distances. On the other hand, it is possible to focus the lower energy and up to about $\pm 15\%$ energy spread beam with solenoid magnets which are more forgiving than quadrupole magnets. For this reason the first two accelerating structures as well as the injector will be immersed in solenoidal magnetic field.

The best way to transport low energy beam to the user is to introduce a bend magnet at the low energy end of the machine to bend the beam to the low energy experiments, using only one accelerator klystron and the structure(s) associated with it. In this scenario the beam will impart energy only to the first accelerator section(s) and so less beam loading compensation will be necessary. Also since almost all of the energy must be achieved from one accelerator klystron, the power into the structure can be increased compared to using the entire complement of the klystrons and structures, and thus the beam loading to final beam energy ratio is further diminished. A final attractive feature of using only the front section(s) of the machine to achieve the low beam energy and bending the beam to the low energy experiment immediately afterwards is that since the first section(s) will be immersed in solenoidal field which is much more forgiving on energy spread than the quadrupoles downstream, thus the low energy, and larger energy spread (as much as $\pm 15\%$) of the beam can be tolerated.

All of the considerations described in this section are achievable with care, based on our experience on much more difficult beam parameters for high energy physics and photon science users. All necessary detailed considerations will be addressed in Phase 2, the to-build design phase of the RPI linac upgrade. The basic machine footprint offered in this report includes preliminary consideration of these issues.

Conceptual Design for New RPI 2020 Linac

In this section we present a conceptual design that meets all the desired operational modes detailed in the previous section. As part of this study we examined three design options for the speed-of-light accelerator sections all of which would be powered by RPI's chosen Thales TV 2022D klystrons. This section begins with a discussion of these three options to provide BMPC-KAPL and RPI with sufficient information to select the one that best meets their goals. Following this discussion are the details on the other major components (injector, buncher, gun, modulator and diagnostics) which are unaffected by the choice of speed-of-light accelerator structure. These options include:

- Option 1 - Eight large aperture traveling wave (TW) accelerator sections powered by four klystrons which meets all the operating scenarios.
- Option 2 - Three long TW accelerator structures with smaller apertures than the structures of Option 1, powered by three klystrons. This option meets most of the desired operating parameters but requires klystrons running at maximum capacity in many cases.
- Option 3 - Three parallel-fed novel standing wave (SW) cavity accelerator structures with even smaller apertures fed by 3 klystrons with some overhead in the klystron power.

While it requires an additional klystron and modulator than the other options, Option 1 is the lowest risk option since it has the largest apertures and most overhead in klystron power for the various operating scenarios. Larger apertures mitigate operational risk because the beam stay-clear will be larger so beam transmission would be easier to maximize and it reduces potential for deleterious wakefields effects. Long range wakefields are known to cause beam breakup instability (BBU) when the image charges on the walls from the front part of the pulse affect the bunches in the back part of the pulse. BBU limits the pulse current and pulse length. Detailed wakefield and BBU calculations are beyond the scope of this study, however, in the proposed Phase 2 program detailed wakefield calculations will be conducted when designing the rf structures for the chosen linac option.

The first accelerator structure design option (Option 1) we examined is a low technical risk approach based on an L-band Traveling Wave (TW) structure designed at SLAC for the International Linear Collider (ILC) positron source [3]. The structures were slightly modified from the existing design to meet RPI's specific requirements. For this design approach, four klystrons (assumed to be Thales TV 2022D), each powering a pair of short (2-m) structures, are required for the accelerator. The available power is sufficient for all modes of operation and is enough to achieve very good beam loading compensation of ± 0 to $\pm 5\%$ in most cases. While beam energy spread is not an important parameter for the end user of the linac, a large energy spread can lead to excessive beam interception in the accelerator sections. For the low energy scenario, the worst-case energy spread is less than $\pm 12\%$. However, the solenoidal focusing used in the low energy region is quite forgiving and can adequately control the beam for this level of energy spread. Further details for this option are described in the latter part of this section.

The second design option (Option 2) is also based on a TW accelerator approach but designed for optimal use of rf power. This option requires only three klystrons, each powering a long (5.15

m) structure, and requiring the maximum available klystron power for most of the desired operational modes. The reduction in the klystron count and associated modulator would provide significant savings. However, the optimal design does have several deficiencies compared to the four-klystron design option. They are:

- This scenario requires the klystrons to run at their maximum peak power for most operating scenarios. It means that all the klystrons must meet their maximum specifications. We recommend a survey of various users of the Thales TV-2022D klystron be performed to determine whether the klystrons reliably operate at their maximum specification.
- For the high average beam power (45kW) operation mode the beam energy will be limited to approximately 140 MeV. The beam loading compensation would vary from ± 3 to $\pm 10\%$ for most cases, though for the low energy case the pulse current would be limited to 4.5 A to keep the energy spread below $\pm 15\%$.
- The length of the accelerating structure could present some difficulty in its construction, such as the so-called 'book-shelving' effect (the cumulative effect from a slight tilt of the cells), when brazing a large number of cells into one structure. Splitting the structure and using two of them per klystron can mitigate this problem, though at the expense of requiring two extra couplers.
- The accelerating structure has smaller iris diameters than the first option, causing it to be more prone to BBU. The detailed calculations to see if these effects are show-stoppers for this structure would need to be done early in the design stage in Phase 2 if there is interest in choosing this structure.
- If the detailed calculations show that the apertures are too small, then we would have to divert effort to the four klystron larger aperture accelerator scenario. If these structures proves to be not usable for RPI 2020 linac, then an additional approximately \$80,000 and an additional 3 months will be needed to revert back to the 4 klystron scenario.

For the above reasons, it might be necessary to make additional funding and time available in phase 2 to revert back to the larger aperture structure design of Option 1 if this does not prove to be a viable design, or if more operational flexibility is deemed important down the line. The attractive thing about this option however is the cost saving due to the reduction of one klystron and associated modulator. Details of this design option are described in Appendix A.

A final design option (Option 3) that was investigated uses a novel SW accelerator option based on recent SLAC accelerator R&D where the cells are powered in parallel through an external coupler. The structure design is highly efficient and only requires three klystrons operating well within their rated power levels to achieve the requirements of the new RPI 2020 accelerator. However this design has the smallest aperture diameter of the three options and will be the most sensitive to beam quality degradation affecting the current transmission. In addition, a structure of this type has not yet been experimentally proven. SLAC has a plan to construct and test a prototype of this structure in X-band (11.424 GHz) in the fall 2014 with test results expected by May 2015. Qualifying these structures for RPI would require construction of an L-band prototype to be tested at SLAC as part of the cost of the RPI design program. It should be noted

that designing, building and testing the L-band prototype is estimated to have a cost of \$900K. Details for this approach are presented in Appendix A.

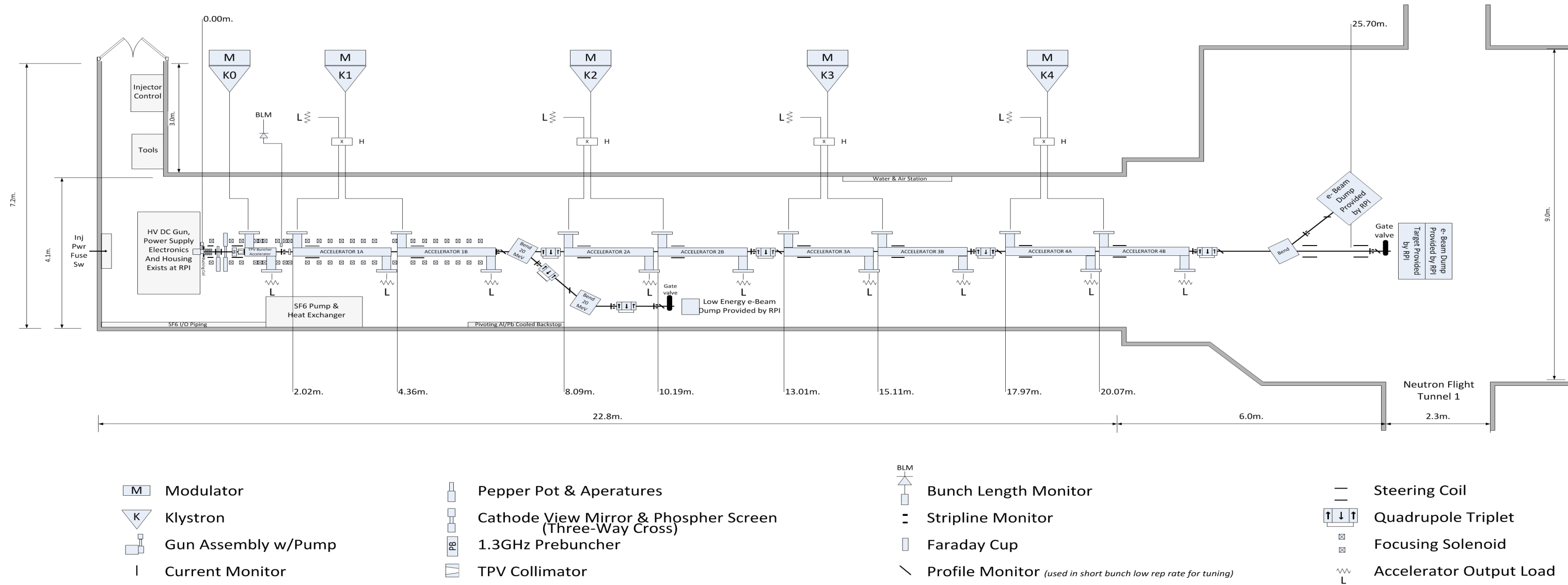
In all three of our design explorations we have attempted to keep the overall active acceleration length to ≤ 16 m to allow room for diagnostics and magnetic optics in the linac up to the neutron target as well as the option to add a bunch stacking beamline at the end of the accelerator if it is desired. It is important to note, however, that in all three of our scenarios the linac without the bunch stacker meets the short bunch (< 6 ns, ≥ 7 kW) electron beam requirements. The conceptual design of a bunch stacker suitable for use at the RPI facility is shown in Appendix B. A detailed design of a bunch stacker which can be installed at RPI is not currently in the scope of the proposed Phase 2 program where the linac from the gun to the target will be designed in detail.

A block diagram of the Option 1 conceptual design of the entire accelerator is shown in Figure 2. The five main areas of this linac are: the injector, the accelerator, the beam line to the low energy experiments, and the high energy beam line to the neutron target. The Option 1 design has another advantage over the other two as it accommodates smaller energy spread in the low energy operation mode, important for maximizing the current transmission to the low energy target. This occurs because the beam at the low energy bend that is placed after the structures powered by the first accelerator klystron has a 40 MeV unloaded energy level in Option 1 (versus the 55 or 75 MeV level of design options two and three, respectively), thereby resulting in the best beam loading compensation and the maximum possible pulse current for an approximately 20 MeV output beam.

Injector

The injector consists of an electron gun to produce the electron pulses at the needed pulse width and repetition rate, a 1.3 GHz single cell pre-buncher, and a tapered phase velocity (TPV) buncher/accelerator section to bunch and accelerate a train of bunches within the pulse such that they occupy $< 40^\circ$ of the accelerating rf field. The beam exits the injector at the speed of light immersed in a solenoidal magnetic field for transverse beam control. In addition, there is a set of diagnostics to tune and evaluate the beam exiting the injector and entering into the first accelerator section. These diagnostics are critical in the injector because there are many tuning parameters (Gun HV and current, bunching fields and phases, several solenoid strengths) and characterizing the beam behavior as completely as possible while these parameters are adjusted is part of the effective machine set-up procedure. The injector also includes vacuum pumps and machine diagnostics to evaluate the state of the machine itself, such as a port to view the cathode and measure its temperature and ion gauges to evaluate the vacuum level where there are no pumps. Figure 3 shows a block diagram of the basic injector followed by the first pair of accelerators that are powered by the first accelerator klystron and the bend to the low energy experiments.

RPI 2020 L-band Linac



Drawing Last Revised: October 23, 2014

Figure 2. Layout of conceptual design for new RPI 2020 Linac

RPI 2020 L-band Linac Low Energy Portion

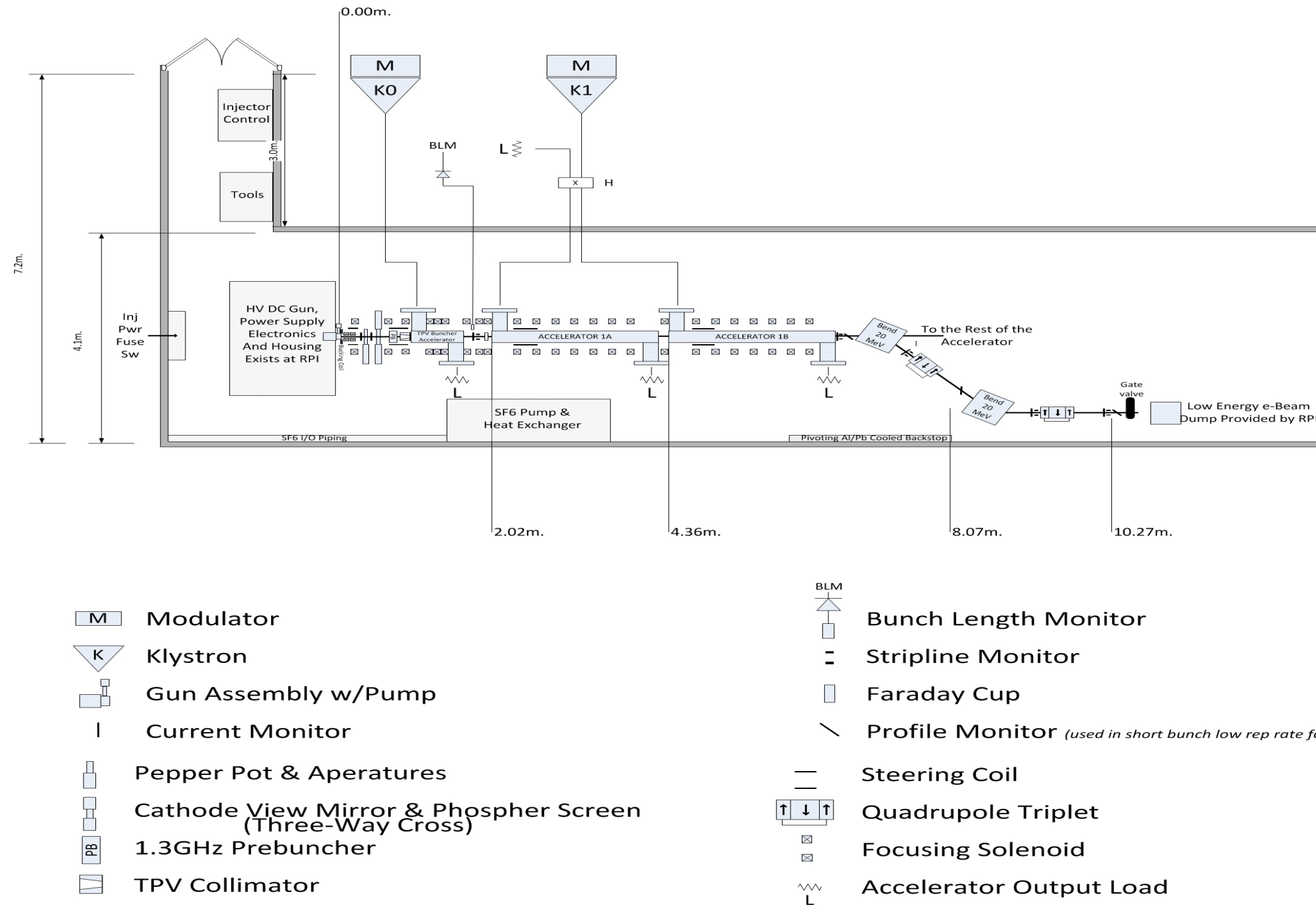


Figure 3. Linac injector, first two accelerator sections and beam line to the low energy experiments.

Given the wide range of desired beam energy operations, it is very important to make the tuning of the injector independent of the tuning of the remainder of the accelerator. In this way, as the overall machine energy is varied to accommodate the various experiments that have about the same pulse current, the injector will not need to be re-tuned. Only minimal injector tuning will be needed for large changes in pulse currents.

The injector tuning parameters depend somewhat on the electron beam current because of space charge and beam loading in the TPV buncher/accelerator. In order to minimize the amount of injector tuning necessary between various operating scenarios for the wide range of experiments at RPI, we suggest powering the TPV buncher/accelerator with its own klystron, independent from the power of the rest of the accelerator. This can most likely be a lower power klystron (approximately 10 to 20 MW peak power) than the Thales TV 2022D klystrons used for the accelerating structures. A more complete recommendation for the klystron to power the TPV buncher/accelerator will be given after the detailed design in Phase 2 of the project.

In principle the TPV buncher/accelerator of the injector can be powered by the same klystron as the first accelerator section to save costs. However, doing so requires a high-power mechanical phase shifter and attenuator placed in the arm of the klystron feeding the TPV buncher/accelerator. The settings of the high-power phase shifter/attenuator will depend on the phase and amplitude of the klystron itself, normally set to accommodate the energy gain needed in the first accelerator section. These mechanical phase shifters and attenuators have mechanical hysteresis and do not always produce the same result when returning to previous settings. This adds more complications for establishing a set of tuning parameters for quick selection of a given set of beam requirements. In addition, these high power mechanical moving components are costly and prone to other complications, such as multipactoring and rf breakdowns. Finally, there is insufficient power from the accelerator klystrons to simultaneously provide power for the TPV buncher/accelerator and still achieve the required beam energy, energy spread and average power for some of the beam operating scenarios.

Ideally, all the rf devices will be fed by their own independent power sources. There are smaller scale rf drivers to drive the prebuncher and typically a coaxial feed is practical for these structures. The power required for the prebuncher will be determined during the detailed design in Phase 2 of the project.

Electron Gun

For the short pulse operation mode (highest priority), the accelerated current to the neutron flight tunnel hall needs to be as much as 14 A. Assuming about a 75% current transmission from the gun to the neutron flight experiments, the gun needs to produce 18 A or more in a pulse. The RPI electron gun is a modified version of the SLAC CID thermionic gun [4], shown in Figure 4, which has a 2 cm² area cathode and was designed to run at 150 kV with a peak space charge limited current of 16 amps, not including the grid interception. The original EGUN [5] simulations of this gun that predict this current are shown in Figure 5. Electron guns derived from the SLAC gun design have and continue to run successfully at up to 150 kV levels at SLAC, Boeing, CERN and in other laboratories around the world. The RPI gun has a slightly different A-K gap geometry and a 3.1 cm² cathode. Simply scaling from the SLAC CID gun indicates

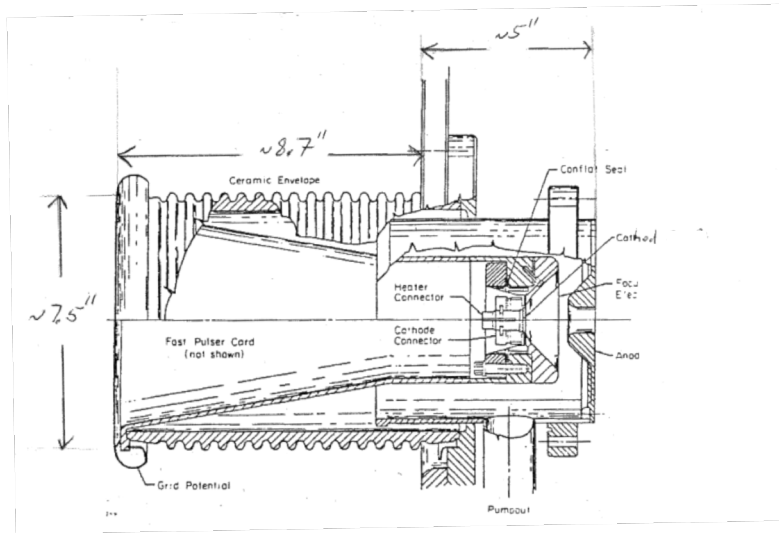


Figure 4. Gun geometry based on the SLAC CID gun design.

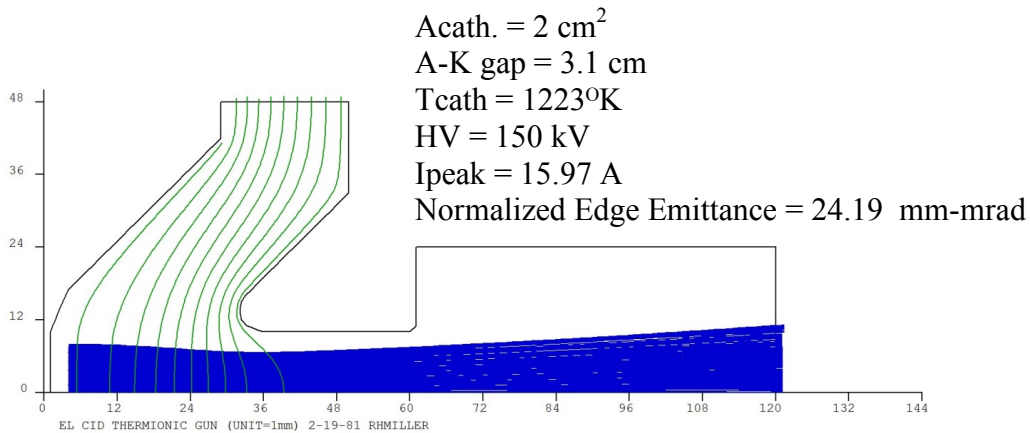


Figure 5. EGUN simulation ray trace and summary of results of the SLAC CID thermionic gun with a 2cm^2 cathode.

that as much as 25 amps is possible from the RPI gun at 150kV operation. According to the cathode manufacturer 30% of this current will be intercepted in the grid leaving 17.5 amps to exit the gun.

We expect the RPI gun, with its 3.1cm^2 cathode, to produce the 17 to 18 A pulse and $< 0.5 \text{ mA}$ average current for the experiments requiring the highest peak and average currents. Experiments are underway at RPI to verify that the existing gun is capable of meeting the required high voltage and current specifications, however simulations of the expected performance of this gun are not found, though some results of simulations are available at RPI. It is necessary to perform those gun simulations in order to first verify that the current electrode geometry of the gun is capable of producing the required current or offer modifications to the anode cathode gap distance and possibly electrode shapes in order to produce the required current. These simulations are also necessary in order to offer a complete set of necessary beam parameters as input to the injector for the various operating scenarios. RPI has provided drawings of the gun with its current A-K geometry and detailed simulation of the RPI gun will be conducted as a matter of first priority in the design-to-build phase of the project.

Another important consideration is the average beam power dissipated on the cathode grid. The cathode used for the RPI gun is the commercially available EIMAC YU 156 cathode. This cathode was originally developed for the Boeing high average power FEL experiments in the 1980s.

Table 2 shows the specifications of the YU 156 cathode. The highest average power dissipated on the cathode grid would be in the long pulse mode of operation. Assuming an absolute worst case scenario of 4 μ s pulse length, 1 A current, at 600 Hz repetition rate from the gun, and all of it being deposited on the grid (typical values are about 30% deposition on the grid), the average current would be 2.4 mA, well below the maximum DC current rating of 550 mA for this cathode grid. Assuming a maximum grid bias of 150V, the power dissipated on the grid would be 0.36W. In a recent communication with the manufacturer, they stated that the cathode grid is rated for up to 4 W dissipation, well above the 0.36 W worst case expected operation at RPI.

Table 2 Specifications of the EIMAC cathodes. The RPI gun employs the YU 156 cathode shown on the last line.

TYPE NUMBER	Cooling ¹	FILAMENT		CATHODE		CONFLAT Size, in.	D _{GK} , microns	MAXIMUM RATINGS			EMISSION	
		Volts	Amps	Area, sq. cm.	Type ²			E _a , V	E _c , Vdc	I _a , mA dc	E _c , Vdc	Ib, Amps
Y-809	A/CC	6.0	1.3	0.1	D	2 3/4	135	6.3	-150	50	6.0	0.003
YU-180	A/CC	6.0	1.3	0.1	D	2 3/4	150	6.6	-150	50	150	0.25
Y-646B	A/CC	6.0	1.4	0.5	D	N/A	150	6.3	-150	50	150	0.75
Y-845	A/CC	6.0	1.4	0.5	D	2 3/4	140	7.5	-150	25	100	1.25
Y-646E	A/CC	6.3	2.2	1.0	D	N/A	150	6.6	-200	75	100	3
YU-171	A/CC	6.3	2.2	1.0	D	2 3/4	160	7.5	-150	25	100	3
Y-646	A/CC	6.3	1.3	0.8	O	N/A	150	6.6	-150	45	180	10
Y-796	A/CC	6.0	5.8	2.0	D	3 3/8	170	7.5	-150	50	100	12
Y-824	A/CC	6.0	5.8	2.0	D	2 3/4	190	7.5	-150	50	200	15
YU-156	A/CC	6.0	8.3	3.0	D	3 3/8	170	7.5	-150	550	100	18

¹ All gun assemblies are forced air and conduction cooled

² O = Oxide Cathode, D = Dispenser Cathode

Bunching System

The electron beam will exit the gun in packets of long pulses ranging from 25 ns to 4 μ s at a repetition rate ranging from 25 Hz to 800 Hz depending on the operating scenarios. The long pulse beam packets, typically referred to as continuous wave (CW), from the electron gun will be chopped into a bunch train with 1.3 GHz spacing by a 1.3 GHz single cell buncher, called the prebuncher. The position of this buncher in the linac shown in the Figure 2 and Figure 3 schematics of the RPI 2020 Linac. This prebuncher will impart a natural velocity modulation on the electrons in the beam, depending on where the electrons fall on the rf wave. The \sim 150 keV CW beam injected from the gun has a constant velocity of \sim 0.63c. The deceleration and acceleration imparted on the beam will be accomplished by the gap voltage of the prebuncher and will be selected based on the best beam dynamics results. Typically the beam energy variation imparted by the prebuncher should be about 10 to 20% of the initial beam energy. The single-cell 1.3 GHz prebuncher should be capable of up to 50 kV gap voltage and can be powered by an rf driver with tens of kW peak rf power. This determination will be made during the to-build design phase of the project. The prebuncher driver should not be a long-lead item and can be ordered soon after the injector design is complete.

As the beam drifts in the post-prebuncher region, the particles with higher energy will catch up with particles ahead of them that have had their energy reduced due to being in the decelerating portion of the rf field, and the beam will begin to form bunch packets. These bunch packets will then enter the Tapered Phase Velocity (TPV) buncher/accelerator to be further bunched and accelerated. The drift distance between the prebuncher and the TPV buncher is strategically chosen. While the electron beam energy modulation due to the prebuncher gap voltage causes the beam to bunch, the space charge forces cause it to debunch, and there is a natural focal point distance where the bunch length is at a minimum. After this point the beam begins to debunch due to space charge forces, unless the beam is further bunched and accelerated by the next rf structure. The TPV buncher/accelerator is placed at or near this focal point.

The TPV buncher/accelerator will be a multi-cell structure whose cells are short in front and gradually increase in length to synchronize with the beam's changing velocity, until the beam gains enough energy that it is traveling at nearly the speed of light. The final few cavities of the TPV buncher/accelerator will be at the speed of light. The phase of the TPV buncher/accelerator with respect to the incoming beam is adjusted to decelerate the leading particles in the bunch and accelerate the trailing particles so that further bunching occurs while increasing the mean velocity and energy of the bunch such that it is traveling at nearly the speed of light by the exit of the TPV buncher accelerator and is energetic enough to minimize the effects of the space charge forces. The rate at which the cell lengths increase depends on the rate with which the beam gains energy. The drift distance between the TPV buncher/accelerator and the first accelerating section is also of strategic importance because of continued slight bunching action and space charge effects that are not yet completely negligible. The beam will exit the TPV buncher/accelerator with ~5 MeV energy with ~500 keV single bunch energy spread. At 5 MeV, the electron beam is already traveling at nearly the speed of light, and the following accelerator sections can be identical to each other.

An example of a TPV buncher/accelerator section, built for Boeing's 120 MeV L-band linac for High Average Power FEL experiment [6], is shown in Figure 6. A similar TPV buncher/accelerator will be designed specifically suited for the new RPI 2020 accelerator during the design-to-build phase.

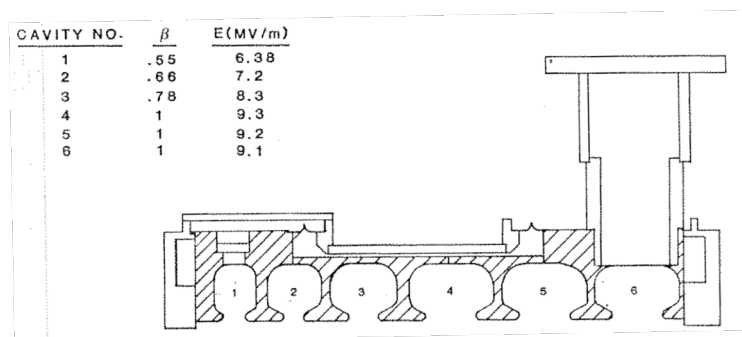


Figure 6. The Boeing L-band TPV TW buncher/accelerator in their 120 MeV linac for High Average Power FEL experiments

Injector Magnetic System

The entire injector system will be immersed in a solenoidal magnetic field to control the beam transverse dimension. This magnetic system will include gun lenses, which will need to be as close to the anode as possible to control the beam growth in the transverse direction yet will need to have a short reach to minimize magnetic field on the cathode where the electrons are generated. The angular momentum imparted on the beam at the cathode with magnetic field at the cathode cannot be compensated will deleteriously effect the beam emittance and hence reduce the beam-stay-clear downstream. The strength of these solenoids will be around 20 Gauss over a 20 cm extent. As the beam enters and exits the field of a given solenoid, the angular momentum imparted on it at the entrance is cancelled at the exit. The gun lens system will include a bucking coil to assure zero magnetic field on the cathode, as shown in Figure 2 and Figure 3 in the injector layout. This bucking coil needs to be strong enough to cancel not only the fields from the gun lenses but also the fields from the large solenoids around the entire injector, which have higher strength and longer reach. The superposition of the fields from the large solenoids facing the injector will be low in the front end (~20-30 Gauss) and quickly ramp to as high as 1200 Gauss over the TPV buncher/accelerator, where it must compensate for increasing space charge forces pushing the beam in the radial direction due to bunching as well as radial electric fields from the rf.

SLAC is in possession of the basic specifications for these magnets as they have been used on various SLAC test accelerator systems. We will employ them in the to-build design phase of the machine possibly with slight modifications.

In addition to the transverse containment of the beam, steering corrector magnets in both the X and Y directions, as shown in Figure 2 and Figure 3, are necessary to keep the beam on the centerline in the injector. Many adverse effects result when the beam is off axis in the injector, such as: the beam changes orbit as the phases of the bunchers are adjusted, the beam changes orbit as the strengths of the solenoids are adjusted, and the beam imparts asymmetric image charges on the rf cavity iris walls, which do not completely cancel and further steer the next bunches in the train. In addition to keeping the beam on the centerline with the steering magnets, the careful alignment of the injector components is crucial. In the design-to-build phase of the project, alignment posts that relate an external accessible portion of the components to their centerline will be included in the drawings and alignment specifications will be part of the specification documentation.

Injector Apertures and Diagnostics

The injector will include diagnostics and removable and permanent apertures in strategic locations, as shown in Figure 2 and Figure 3 (linac layout and the expanded view of the injector and low energy experimental region layouts).

The retractable multiple aperture and pepper-pot system sandwiched between two current monitors after the gun lenses has several purposes. The apertures combined with the beam current reading before and after it will help to tune the beam size at the exit of the gun with the magnetic lenses. Additionally varying sizes of apertures may be necessary to limit the gun pulse current for the very low pulse current operation cases. The pepper-pot, which is basically a plate

with small holes strategically placed at different radii, in combination with the screen downstream is also a useful tuning tool for measuring the beam size at the exit of the gun where there is no room for a screen; it will assure that the beam is traveling as close to the magnetic centerline as possible based on the response of the image of the beamlets on the screen while various components are adjusted. Additionally, if the screen is far enough from the pepper-pot, it will provide a method of measuring the beam emittance at the exit of the gun.

A three-way cross, which includes an insertable profile monitor from one direction and a mirror from the other direction combined with a quartz window at the 90° port from both of them, will allow an operator to check the beam profile with the screen and to view the cathode with the mirror to measure the cathode temperature with an optical pyrometer. This allows the operator to verify that the cathode is being heated to the proper temperature. The beam position and current monitors provide a non-interrupting method of measuring and tuning the beam orbit and current.

The permanent aperture followed by a current monitor at the entrance of the TPV buncher/accelerator will allow the tuning of the magnetic system to assure the beam spot size is not larger than necessary as it enters the buncher/accelerator. This is important because the beam is phased such that it is at or near the zero crossing of the rf in the front cells of the TPV buncher/accelerator where, while the longitudinal electric fields focus the beam in the longitudinal direction, the radial electric fields defocus the off-axis particle in the transverse direction. Thus keeping the beam size as small as possible at the entrance and in the TPV buncher/accelerator is an important consideration.

A very important and inexpensive diagnostic at the exit of the TPV buncher/accelerator and before the first accelerator section is the bunch length monitor. This is a high harmonic (probably third or fourth harmonic) cavity that sits in air near a ceramic gap in the beam pipe. Similar gaps are required for the current monitors. As the beam passes through this ceramic gap in the beam pipe, it induces fields in the bunch length monitor cavity. The rf in this cavity can be transported with a waveguide from the accelerator beam line (out of the shielding walls of the accelerator hall) and measured with a crystal diode and oscilloscope. The magnitude of this signal is proportional at varying degrees to the charge in the bunch, the shortness of the bunch, and distance of the bunch from the cavity. Using the beam position monitors to keep the beam centered on the centerline, then adjusting the bunching elements in the injector to maximize the signal from the bunch length monitor is a very easy, convenient, and highly effective way to tune the injector rf components. This was the typical method used at SLAC for beam tuning for the SLAC Linear Collider experiments.

If space permits, an insertable Faraday cup can be added just prior to the first accelerator section to accurately measure the current out of the injector, where most of the current interception would happen. By the time the beam enters the first accelerator section, almost all the beam losses should have happened and the beam transmission inside the accelerator and beamline systems should be >90%. The overall beam transmission from the gun to the end of the 150 MeV linac is expected to range from 70-75% based on experience with similar designs on various linacs around the world.

Injector Power Sources

Four major rf and electrical power sources are required in the injector: the gun HV power supply, the prebuncher rf driver, the TPV buncher/accelerator klystron, solenoid power supplies, as well as smaller power supplies for the cathode heater, insertable diagnostics actuator motors etc.

RPI will need to confirm the existing gun HV power supply is capable of delivering the required voltage and current to sustain 160 kV, up to 25 A peak current at short pulses (~10ns) and ~1A long pulses (~ 3 to 5 μ s) at ~400 to 800 Hz repetition rate. The gun should be processed up to 160 kV for reliable routine operation at 140 to 150 kV. These values take into consideration some overhead in the power supply capability compared to the desired output from the gun.

The specifications for the magnet power supplies will not be known until the magnet designs are completed but they are likely to be high current (hundreds of amps) and tens of Volt power supplies, depending on how many magnets can be strung in series based on beam dynamic considerations. Magnets requiring the same current could be powered by the same power supply to save costs.

The prebuncher rf driver needs to provide approximately a few tens of kW peak power and less than 100 W average power at 1.3 GHz. The TPV buncher/accelerator rf requirements are approximately 10 MW to 20 MW peak and 15 to 30 KW average power. More specific requirements will be known after the final detailed design of the upgraded machine.

Speed-of-Light Accelerator System

Accelerator Structures

Using the Option 1 design for the main accelerating portion of the linac, there will be eight 2-meter structures powered by four klystrons. The beam exiting the injector system into the acceleration sections will be nearly at the speed of light so it can remain synchronized with the rf in the accelerator. The accelerator structures will be identical, with the rf in these accelerator sections phased such that the beam rides at or near the crest of the rf for maximum energy gain. In the accelerator, the relative energy spread in a single bunch will be determined by the bunch length ($\Delta E/E = 1 - \cos(\theta/2)$), where θ is the bunch length in degrees or radians of the accelerating rf. The beam loading in the accelerator will determine the total energy spread of the entire pulse. Even though the experiments envisioned for the RPI linac are very tolerant of large energy spreads, it is important to minimize both the single bunch energy spread and the total pulse energy variation as much as possible in order for the beam to be manipulated uniformly by the magnetic optics in the accelerator. The beam energy at the exit of the first two accelerator structures powered by the first high power klystron will be approximately 40 MeV in most operating scenarios and less than that for the low energy operating scenarios. The rf power from the first accelerator klystron K1 (shown in Figure 2 and Figure 3) will be phased such that the beam is slightly behind the rf crest so as to remove as much of the energy spread remaining in the beam bunch as a result of the ballistic bunching.

Figure 7 shows the first, middle, and last cells of the Option 1 proposed structure design including the modeling mesh. A variable modeling mesh is chosen to assure a fine mesh on the small curves for accuracy and not so small but sufficient mesh size in other areas for modeling speed. One can see by examining the cavities in Figure 7 that while the cell length and aperture sizes are kept constant, the gap between the iris noses is reduced (and the iris thickness increased), giving the illusion of the cells becoming shorter toward the end, though this is not the case. In order to mitigate beam break up, single bunch wakefield, and beam stay-clear issues, the accelerator cells' iris apertures are designed to be as large as possible. To maintain a near constant gradient throughout the structure while also maintaining larger iris aperture size the outer wall of the cells is rounded and nose cones are introduced at the irises to increase the shunt impedance of the structure. The gap between the noses is reduced gradually from the front to the end of the structure to maintain the constant gradient feature without reducing the aperture size toward the end, where less power per cell is available than in the front of the structure. The parameters of the Option 1 accelerator structure are shown in Table 3 and Table 4 lists the expected beam parameters and needed klystron power for various modes of operation to serve the enhanced experiments at RPI. There is good margin between required rf power and that available from the klystrons. The maximum energy variation between the first and last bunch ($\sim\pm 12\%$) occurs for the low energy, high current experiments. In this operating scenario only the first two accelerating structures are used. Those accelerator sections have solenoidal focusing magnets that have a higher beam energy spread tolerance than quadrupole magnets. In this Option 1 linac scenario with eight accelerating sections powered by four klystrons, the electron beam energy variation for the high energy operating modes is $\pm 5\%$ or less. The quadrupole magnets which are used to control the beam transverse size beyond the second accelerating section can easily accept this level of beam energy variation. It is not practical to use solenoids for the transverse containment of the beam beyond the first two accelerators as the beam energy is so high that very large and complicated solenoid magnets would be required to guide the beam, hence the switch to quadrupoles and the more stringent requirement on beam energy spread downstream of the second accelerator structure.

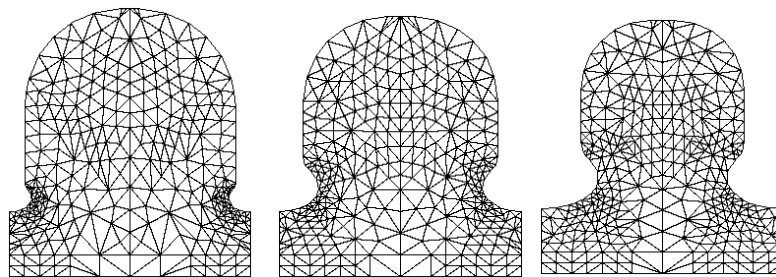


Figure 7. The first, middle and last cells of Option 1 constant gradient TW accelerator with constant aperture throughout the structure and variable modeling mesh size to assure an accurate representation of the small curves.

Table 3 Structure parameters for the Option 1 traveling wave (TW) structure design of the upgraded RPI 2020 accelerator.

Frequency	1.3 GHz
Structure Type	TW $5\pi/6$
Number of Cells	21 (2m)
Aperture 2a	4.6 cm
Attenuation τ	0.5
Q	25872 - 22301
Group velocity V_g/c	0.37% - 0.12%
Shunt impedance r	46.34 to 36.37 M Ω /m
Filling time T_f	2.9 μ s

Note:

- a is the radius from the centerline to the iris of the accelerator structure. 2a is the bore diameter
- τ is the attenuation factor relating Power out vs Power in by the following expression:
 $P_{out}/P_{in} = \text{EXP}(-2 \tau)$
- Q is the Quality factor of the cavities in the structure indicating how rapidly the stored rf energy is dissipated. The higher the Q, the slower the dissipation.
- V_g is the group velocity of the rf in the cavities of the structure indicating how quickly the structure is filled. It is expressed in units of percentage of the speed of light, c.
- r is the shunt impedance of the cavities in the structure per unit length indicating the accelerating quality of the structure. The higher the shunt impedance, the less power is needed.
- T_f is the time needed to fill a traveling wave structure. After one filling time, the structure empties as quickly as it fills and is considered to be in steady state.

Table 4 Major electron beam parameters and rf power requirements for the upgraded RPI 2020 accelerator Option 1 scenario utilizing 2-m, Constant Gradient, TW accelerator structures.

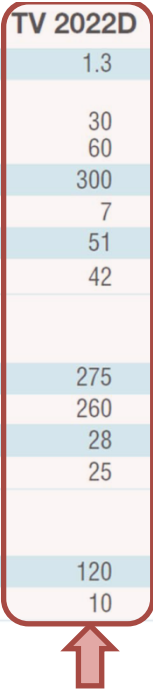
No. Struct. / No. Klys.	Total Active Acc. Length (m)	Operating Mode	Beam Injection Time (ns)	Beam Pulse Len. (ns)	Beam Accel Pulse I (A)	Ave. Beam Energy (MeV)	$\Delta E/E$ (%)	Rep Rate (Hz)	Beam Ave. Power (kW)	Peak RF Power (MW)	Ave. RF Power (kW)
8 / 4	16	Short Pulse	3200	5.4	13	148	± 1.3	700	7.3	16.2	36.3
8 / 4	16	Low Rep Rate	3200	250	1.6	143	± 5	25	1.4	25.6	2.2
8 / 4	16	High Power	2050	1667	0.45	145	± 3	413	44.9	24.8	38.1
8 / 4	16	High Power	2050	3000	0.45	145	± 3	230	45.0	24.8	28.8
8 / 4	16	High Power	2050	4000	0.45	145	± 3	172	44.9	24.8	25.8
2/1	4	Low Energy Max Current	3200	25	10	20	± 12	800	4.0	6.0	15.5
2/1	4	Low Energy Small $\Delta E/E$	3200	25	3	20	± 5	800	1.2	3.4	8.8
2/1	4	Low Energy Long Pulse	2050	250	0.94	20	± 5.9	750	3.5	21.8	37.6
2/1	4	Low Energy Longer Pulse	930	2500	0.9	20	± 7.5	480	21.6	25.6	42.2
2/1	4	Low Energy Longest Pulse	930	3500	0.9	20	± 7.5	400	25.2	25.6	45.4

RF Sources

The linac conceptual design is based on using Thales TV 2022D klystrons whose operation specifications are shown in Table 5. The key rf parameters are: 30 MW peak power, 60 kW average power, and $\leq 7 \mu\text{s}$ pulse length. We assume that 10% of the klystron power is dissipated in the rf waveguide system leading up to the accelerator structure, thus we require that the linac meet the required electron beam operating parameters with $\leq 27 \text{ MW}$ peak, $\leq 54 \text{ kW}$ average available power. Some considerations were given to enhancing the available peak rf power from the klystrons by using a pulse compression system, but this approach proved not to be useful for reasons explained in Appendix C.

Table 5 Thales TV 2022D klystron specifications.

RF performance	TV 2022A	TV 2022B	TV 2022D		
Frequency	1.3	1.3	1.3	GHz	
RF output power:					
• peak	20	20	30	MW	
• average	50	60	60	kW	
Peak RF drive power	250	250	300	W	max.
RF pulse duration	8	10	7	μs	max.
Saturated gain	50	51	51	dB	typ.
Efficiency	42	42	42	%	typ.
Electrical characteristics					
Cathode voltage	239	239	275	kV	typ.
Beam current	199	199	260	A	typ.
Heater voltage	28	28	28	V	max.
Heater current	25	25	25	A	max.
Cooling					
Collector coolant flow			120	l/min	
Body coolant flow			10	l/min	



If we make the reasonable assumption that the modulator pulse rise and fall time is approximately 1 μsec , with a 7 μsec flat top, and that the klystron gun beam power to rf conversion efficiency is 42%, we can calculate the klystron gun average beam power to be 163 kW at the klystron’s maximum rating operation of 30 MW rf peak, 60 kW rf average power. The repetition rate for this mode of operation would be limited to 286 Hz to stay below the 60 kW average rf power limit. In principle the collector should be able to handle the full gun beam power even when there is no rf, as such a condition could occur in case of a fault. For the moment we assume that the klystron collector cooling is capable of handling at least 163 kW, however, during the detailed accelerator design in Phase 2 of the program, we plan to contact Thales to find the collector power rating. Table 6 shows calculated klystron gun high voltage and current that would be used for various operating modes of the linac. It shows the expected klystron gun beam power for the various operating modes of the RPI linac are all lower than the estimated klystron gun maximum beam power.

Table 6 Thales TV 2022D Klystron Gun Beam Operating conditions for the various Option 1 RPI 2020 Linac Operation Modes.

Beam Oper. Modes	RF Pulse Length (us)	Rep Rate (Hz)	Peak Power @ Acc. (MW)	Ave. Power @ Acc. (kW)	Klystron RF Peak Power (10% more) (MW)	Klystron RF Peak Power (10% more) (kW)	Kly Gun Vo (kV)	Kly Gun Io (A)	Kly Gun Beam Peak Power (MW)	Kly Gun Beam Ave. Power (kW)
Short Pulse	3.205	700	16.2	36.4	17.8	40	231	200	46.2	144.9
Low Rep Rate	3.450	25	25.6	2.2	28.2	2.4	269	252	67.8	8.2
High Power	3.717	413	24.8	38.1	27.3	41.9	275	260	71.5	139.3
High Power	5.05	230	24.8	28.8	27.3	31.7	275	260	71.5	99.5
High Power	6.05	172	24.8	25.8	27.3	28.4	275	260	71.5	86.7
Low E High I	3.225	800	6	15.5	6.6	17.0	189	149	28.2	97.9
Low E Small $\Delta E/E$	3.225	800	3.4	8.8	3.7	9.7	179	136	24.4	82
Low E Long Pulse	2.3	750	21.8	37.6	24	41.4	262	241	63.2	156.3
Low E Longer Pulse	3.43	480	25.6	42.2	28.2	46.4	279	265	73.8	157.0
Low E Longest Pulse	4.43	400	25.6	45.4	28.2	49.9	279	265	73.8	160.4
Klystron Max Power and Pulse Width	7.000	286			30	60.1	275	260	71.5	163

Modulators


As shown in the Thales TV 2022D specifications (Table 5) the efficiency of the TV 2022D klystron is 42%, the peak cathode voltage is 275 kV, and the peak cathode current is 260 A. To power this klystron for the Option 1 accelerator design with sufficient operation margin, the modulator needs to provide 75 MW peak and 170 kW average power. In addition, the modulator must be able to provide a high voltage flat-top of up to 7 μ s.

One catalog item modulator that meets the peak power requirement is the K2-4 modulator from ScandiNova. The specifications of this modulator as well as a few other high power modulators from the ScandiNova catalog are in Table 7.

Limiting the modulator average power to 100kW (as is the case for the ScandiNova K2-4 modulator) places severe constraints on the maximum achievable pulse repetition rate for a given rf peak power and pulse width. This is demonstrated in Figure 8 which is a set of curves that show the allowed repetition rate vs pulse length for a given peak rf power from the klystron assuming that 100 kW average power is available from the modulator. The higher the desired peak power, the lower the allowed repetition rate is for a given pulse length. Thus the repetition rate vs. pulse width for the 30 MW peak klystron rf power is the lowest curve and the repetition rate vs. pulse width for the 15 MW peak klystron rf power is the highest curve in the graph. All the allowed repetition rates for the modulator must fall below the respective high peak power curves. The symbols in the graph indicated the worst case in each operating scenario which RPI wishes to have and the required peak power for those scenarios. As an example, for the high power experiments (the purple triangle) where 45 kW average beam power is achieved with the klystron operating at 27.3 MW peak power, 3.7 μ s pulse width (fill time + beam pulse length), and 413 Hz repetition rate (line three of Table 6), the K2-4 modulator falls short of allowing the necessary repetition rate. (See the relationship of the purple 30 MW peak rf power curve and the purple triangle symbol on Figure 8.). Similarly the short pulse and some instances of the low energy operation repetition rates fall above their respective peak power curves. (See the red hexagon and purple circle for the short pulse and low energy operations respectively.)

Table 7. ScandiNova catalog modulators K2-4 specifications meet the peak power but not the average power specifications for the new RPI 2020 accelerator.

K2-Series



Parameters	K2-1	K2-2	K2-3	K2-4	Unit
RF Peak Power	15- 30	25 - 40	30- 60	50 - 90	[MW]
Pulse Voltage	200 - 265	250 - 330	280 - 450	0 - 450	[kV]
Pulse Current	180 - 265	200 - 350	230 - 450	0 - 500	[A]
Modulator Peak	74	92	160	240	[MW]
Modulator Avg.	0,5 - 54	0,5 - 72	0,5 - 100	100	[kW]
Mains: 1 / 3 phase	3	3	3	3	
Cooling	water	Water	Water	Water	

75MW Peak 100 kW Average Power Modulator

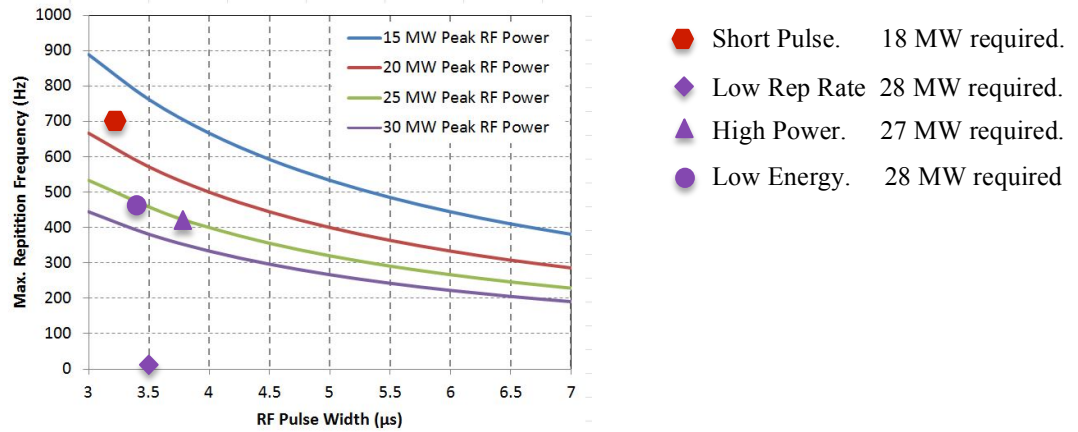


Figure 8. Maximum allowed repetition rate vs pulse width for a given klystron rf peak power for the ScandiNova K2-4 modulator

To assure that the modulator is not the limiting factor for the experiments envisioned at RPI, a 75 MW peak and 170 kW average power modulator is needed. In this case, the maximum possible pulse repetition rates for a given pulse width and peak rf power for the worst case in each operating scenario are shown in Figure 9. Using the same case as an example: high power experiments, where 45 kW beam power is achieved with the klystron operating at 27.3 MW peak power, 3.7 μs pulse width, and 413 Hz repetition rate (line 3 of Table 6), this modulator can now comfortably provide the needed pulse repetition rate. (See the relationship of the purple triangle with respect to the purple 30 MW peak rf power curve in Figure 9.). The other operating points fall well below their respective peak power curves.

75MW Peak 170 kW Average Power Modulator

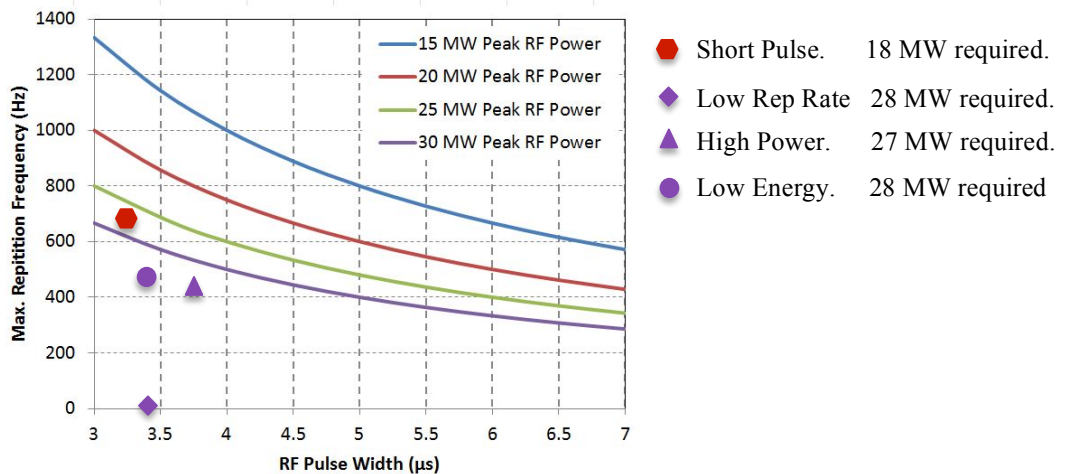


Figure 9. Maximum allowed repetition rate vs pulse width for a given klystron rf peak power for a 170 kW average power modulator

While the ScandiNova catalog item K2-4 modulator meets the peak power requirements, it does not meet the average power requirement, however the modulator requirements for the new RPI 2020 L-band accelerator are not too far away from the K2-4 specifications. There are several commercial modulator manufacturers that have produced systems with similar specifications as needed for RPI, and all of them (including ScandiNova) build to the customer's specifications. We recommend requesting bids from several companies to build the modulator based on specifications required for the accelerator. The modulator is not viewed as a high risk item to the project. While selecting the modulator is not part of SLAC's scope of work for the RPI 2020 linac, we have an extensive modulator expertise at SLAC and would be glad to review the modulator specification document prepared by RPI prior to bid requests.

Magnetic Focusing and Steering

A spectrometer bend after the first two accelerator sections following the TPV buncher serves a dual purpose when activated: 1) It will bend the beam toward the low energy experimental beamline, and 2) it will allow energy and energy spread measurements of the beam after it has been bunched in the injector and its energy spread compensated by the first two accelerating structures. The existing low energy bend magnet at RPI will probably fit this purpose. If not, a bend magnet suitable for this purpose might become available from the SLAC 3-km accelerator within the next two years in preparation for the LCLS II installation in the first third of the SLAC tunnel. This magnet can become available to RPI for the cost of its removal and transport. However a second bend magnet is also needed at the low energy beamline to make the low energy experimental station parallel to the linac. It is best to make these two bend magnets identical and power them in series. The focusing between the bends and upstream of the target could be very large bore quadrupoles or possibly solenoids to be determined in the detailed design phase. In the diagram we show quadrupoles.

The first two accelerating sections are immersed in a solenoidal magnetic field because the beam energy in this region is low enough that reasonably sized solenoids can work here and the energy spread in this region is the highest. As mentioned above, solenoidal focusing has a large beam energy spread acceptance (approximately $\pm 15\%$). Downstream from the accelerator sections powered by the first klystron, the beam transverse size will be controlled by magnetic quadrupole triplets between each pair of accelerator sections powered by a single TV 2022D klystron (see Figure 2). These triplets will have enough strength to focus the beam to a waist in the center of the accelerating length powered by each TV 2022D klystron. The strength of these quadrupole triplets will vary from $\sim 5\text{T/m}$ to about $\sim 10\text{T/m}$, their length will be about $\sim 10\text{ cm}$ for the outer magnets and 20 cm for the center magnet, and their pole-face to pole-face distance will be $\sim 5\text{cm}$. Similar quadrupoles will become available during the dismantling of the first third of the SLAC accelerator in preparation for the LCLS II installation. The specifications for these magnets will become available shortly after the linac design and can be used to go for bid for their construction.

Another 30° bend magnet at the end of the linac will bend the beam toward the energy analyzing leg when it is desired to tune and determine the electron beam energy. During normal operation this bend magnet is de-energized and degaussed. A magnet suitable for this purpose might also become available for the cost of dismantling and transporting from SLAC in a couple of years.

X and Y pairs of steering coils, as shown in Figure 2, will be used to keep the beam on the centerline of the accelerator. The steering magnets will be designed to best suit the beamline components and drawings will be provided for requesting bids from manufacturers.

A bank of power supplies is needed to power the focusing and steering magnets, to control insertable diagnostic actuator motors, and to remotely insert or retract vacuum valves. Some of these insertion devices can also be pneumatically actuated. The power supplies for the steering coils need to be bipolar. The specifications for all of these power supplies will be given in the to-build phase of the new RPI 2020 accelerator as the systems they will power become defined and specified at the to-build level of detail.

Diagnostics

Current monitors, wire scanner or quartz screen profile monitors, and stripline beam position monitors deployed along the machine, as shown in Figure 2, will allow the monitoring of the beam parameters as the beam travels through the accelerator. These diagnostics will help to achieve reproducible tuning scenarios and machine settings for the many different electron beam configurations delivered to the experimenter. Sometimes, to save costs, the number of necessary diagnostics is reduced in the design and construction phase of a new machine. This typically results in more spending later to add the diagnostics after time and money has been spent in trying to operate without them. Often, because the diagnostics were not part of the initial design process, there is no room or way to add them at key locations where they should have been designed in to start with. Based on our experience, we highly recommend that machine and beam diagnostics not be omitted to save costs in the design and construction phase.

Vacuum, Temperature Stabilization, Machine Protection

Perhaps obvious but worth mentioning is that the machine layout needs to include space for pumps, vacuum diagnostics, and valves in strategic locations of the machine. A machine protection scenario that automatically closes gate valves when the pressure in an accelerator section rises is important for saving the integrity of the entire machine. In the injector, the location of these components is critically coupled with the distances necessary for bunching. In the accelerator there is more freedom to allow space for them. The vacuum level in the gun needs to be better than 10^{-9} Torr, while in the accelerator it can be in the mid to high 10^{-9} to 10^{-8} Torr range.

We are investigating the best scenarios for the waveguide environment. While here at SLAC our S-band waveguides are under vacuum, in the case of L-band waveguides where the volume is four times larger, other considerations such as cost, strength of the walls, bracing, etc. must be included. Our current thinking is that the waveguides will be filled with either dry nitrogen or dry air to suppress breakdown, given that managing SF₆ is a much more difficult issue. A ceramic window between the klystron and the waveguide and the waveguide and the accelerator will separate the pressurized waveguide environment from the vacuum in the klystron and the accelerator. In case of a crack in these ceramics the standard protection will be activated to shut down the klystron and insert the gate valves in the accelerator if a window on the accelerator end is compromised. The accelerator design will also include the design for the load for unused rf

power, however the design of the waveguide run from the klystron to the accelerator input window is left up to RPI as it is highly dependent on the geography of the test chamber and klystron gallery.

If temperature stabilization of the accelerator sections will be needed, it will be designed into the structure in the to-be-built design phase of the machine. The same will be the case for the electromagnets: if they will need cooling, it will be specified in the to-be-built design phase.

Machine protection measures need to be taken, especially for the high average power operating scenarios. Any time an insertable device (diagnostic or valve) is in the beamline, the beam repetition rate needs to automatically reduce to an acceptable level to protect the machine. If the power on these devices exceeds the cooling capacity of that device, it should cause the machine to trip. All temperature controlled systems, such as electromagnets should have klixons which will open the circuit and interrupt the current to the magnet coils when their temperature exceeds the maximum allowed for it. A Panofsky Long Ion Chamber [7] [8] (PLIC) line installed along the accelerator can be used to trigger limiting the machine repetition rate or a machine shut-off when it indicates an excess level of localized radiation due to beam interception by the accelerator pipe or structure walls in the process of steering and the magnetic optics which could cause the beam to scrape on the pipe wall.

Proposed Multiphase Program for RPI Machine Development

We envision a four-phase program for the realization of the RPI accelerator machine upgrade. These phases are: Phase 1 – Conceptual Design, completed with the submission of this report, Phase 2 – Linac design, Phase 3 - Construction and assembly of the new linac, Phase 4 – Commissioning. Continuity and expertise in the successful completion of each phase is critical for the success of the final project. All skill levels and facilities for this effort from beginning to end exist at SLAC and can be available to RPI.

Phase 1: Conceptual Design

In this Phase 1 program that resulted in this report, SLAC was charged with producing a conceptual design of a machine that meets the RPI accelerator users' goals and to estimate the effort for a detailed to-build linac structure and other components design.

Phase 2: Linac Design: Program Plan and Cost Estimate

In a Phase 2 project for design of the RPI 2020 linac (components and assembly) to the drawing stage, about two and a half years of focused effort is needed from a multiple variety of accelerator expertise. Having designed, built, commissioned, and operated large-scale machines with much more difficult beam parameters, SLAC is well suited for the successful completion of Phase 2.

A proposed project schedule for the Phase 2 program is shown in Figure 10. The Phase 2 project is a design only program; no construction is included except if the Option 3 linac structure is chosen. If so, then an experimental prototype verification program would be included as described in Appendix A. Phase 2 of the program assumes that SLAC's responsibility will be to:

- Design the upgraded linac beamline and all of its components including component supports and overall machine supports such as the tables
- Provide engineering drawings of all components that would be custom built
- Provide specifications of components that can be purchased from commercial sources

The planning of the Phase 2 program schedule was devised so the design of the long lead items such as the rf structures (prebuncher, TPV buncher and accelerator sections) would be completed early in the program. Engineering drawings of the rf structures will be delivered to RPI by the end of Year 1, Quarter 1 after project start as indicated in Figure 10. The specifications will include the necessary details to define the power source for the various devices, however the responsibility of selecting those power sources will be RPI's. The design responsibility for transmission lines from the sources to the components on the linac also belongs to RPI and is not included in our effort estimate. This includes the cable tray layouts, considerations of the additional power supply voltage needed to compensate for losses in the cables, and so on. Also not included in the Phase 2 program is design of the control and data acquisition systems and peripherals such as cameras for screens or the oscilloscopes for looking at various beam diagnostics signals. For the items not included in the Phase 2 design, SLAC personnel are available to discuss and provide guidance to RPI at any time during this process.

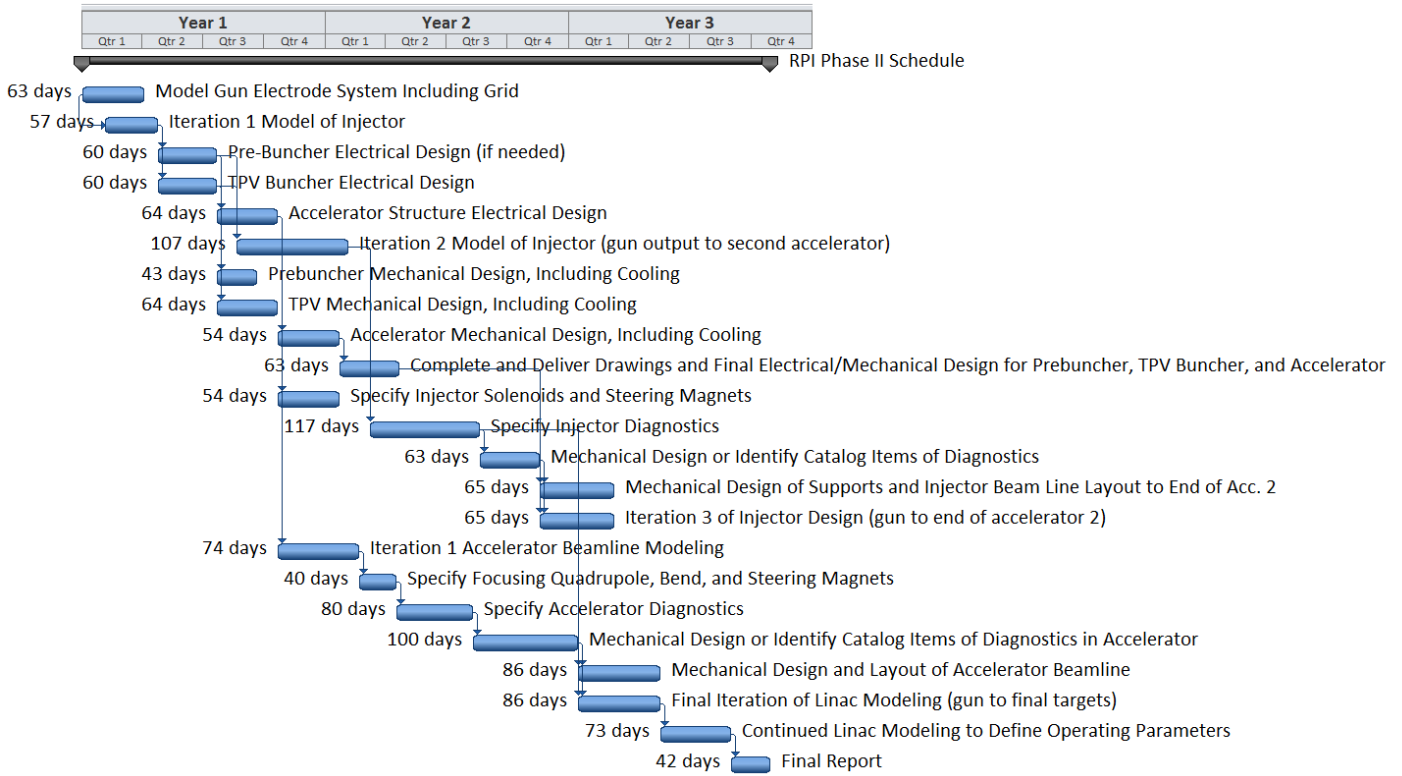


Figure 10 Proposed Phase 2 project tasks and schedule.

Phase 3: Construction Phase

An important component of the construction of the various rf structures is the tuning afterwards. SLAC will be pleased to provide estimates for constructing of the structures. These structures will need to be tuned regardless of who constructs them. Certain diagnostics such as current and position monitors, and beamline components such as electromagnets need to be calibrated. SLAC is probably the best suited to conduct these calibrations at SLAC. In Phase 3 RPI will also assemble the new machine according to the beamline drawings supplied by SLAC in Phase 2. The installation will include alignment, controls, and data acquisition systems. SLAC with its extensive experience in all phases of accelerator design and construction can be a valuable partner to help assure all the proper steps are taken in the construction phase to avoid errors during the commissioning stage and to tune and calibrate the critical components. A rough order of magnitude estimate for some of the mentioned tasks is as follows:

- Tuning eight accelerating structures plus the TPV buncher and prebuncher including making specific supports for the L-band structures as needed – 2 people 12 weeks in a 3 month duration, - \$210K
- Interfacing with suppliers of all beamline components – multiple people for the duration of the construction phase - 1 man-month - \$42K

- Calibrating magnets and diagnostics at SLAC including time spent at RPI – 4 man-months over the duration of the construction phase \$168K
- Travel expenses for three one-week trips to RPI during assembly – \$15K

Phase 4: Commissioning Phase

The final phase of any major upgrade to an accelerator such as is envisioned for the RPI 2020 linac, is the commissioning phase. In this stage the machine is turned on for the first time, component settings are evaluated and fine-tuned starting from design settings; procedures are established for operating scenarios from the first turn-on to after a downtime, to changing parameters for different experiments, to keeping the machine tuned up at its given state. The beam states and strengths of all the machine components are documented for future reference. A rough order of magnitude estimate for participating and consulting in Phase 4 for some of the mentioned tasks is as follows:

- Participate in the pre-turn-on checkout – 2 man weeks – \$42K
- Participate during first turn on and commissioning of the various beam parameters – 3 man-months different people at RPI at different times depending on the commissioning phase over a 4 month period - \$104K
- Travel expenses to RPI - \$35K
- Write detailed, machine specific procedures for each type of operating scenario for future use - \$40K

Once all four phases are completed, the machine is ready for its routine operation to serve the user community.

Summary

SLAC's relationship with RPI has been instrumental in defining the wide range of electron beam parameters for the multiple types of experiments envisioned on RPI's new accelerator using current technology. These parameters range from short pulse (<6 ns) and relatively high power (>7 KW) to long pulse (>1 μ sec) and high power (45 kW) and from low energy (20MeV) to high energy (150 MeV).

In this report, SLAC proposed three viable concepts for the design of the speed-of-light accelerator structures. The concepts range from low-risk, highly-flexible, and robust design to a novel design with very high efficiency that could result in the reduction of one klystron and associated modulator. Of these three design options, the low-risk, four klystrons powering eight 2-m traveling wave accelerating structures option (Option 1) provides the most robust system and can provide the desired beam parameters for all of RPI's envisioned operating scenarios while operating the envisioned klystrons within their operational rating.

The Option 1 accelerating scenario is presented in the main body of the report and is the one that appears in Figures 2 and 3. The other two options are presented in Appendix A. The advantages and disadvantages of each scenario are discussed in their relative sections. The eight-structure, four-klystron scenario meets all beam requirements using Thales TV-2022D klystrons. The three-long-structure, three-klystron version requires the Thales klystrons running at near their peak power limit for most of the operating scenarios in order to compensate for beam loading and falls short of the high current low energy operation specification. It can accelerate up to 4.5 amps with acceptable energy spread but the low energy current specification requirement is up to 10 amps. However if RPI is willing to compromise on the performance of the machine, it could result in savings of the cost of a klystron and modulator. The three klystron version powering parallel-fed standing wave cavities is attractive because it saves the cost of one klystron and one modulator, and the klystrons in this scenario do not need to operate at their maximum capacity for most cases. However, this novel, recently patented SLAC innovation will need to be proven with an L-band prototype that will add approximately \$900K to the initial design cost.

Figure 2 and 3 in this report show a basic machine layout that shows beam optics, diagnostics, and controls that would fit in the existing RPI test chamber. The proposed beam optics, diagnostics, and controls were designed with considerations for the complexity of the wide range of the beam parameters required by the users, a reliable and efficient machine tuning scenario to achieve these parameters, and machine and personnel protection safety measures.

SLAC is well suited for realizing the future phases of the new RPI linac project because of its extensive experience and infrastructure in designing, testing, building, and commissioning large working accelerators to perform according to their expected specifications. This experience will be valuable for realizing the new RPI accelerator from the design phase to completion of the commissioning and preparation for the user base. SLAC would be pleased to participate in all phases of the RPI 2020 linac project at a level most beneficial to RPI.

Appendix A: Alternative Accelerator Designs

In this appendix we provide further details on the Option 2 and Option 3 speed-of-light structures for the RPI upgrade.

High Efficiency Constant Gradient TW Structure for Design Option 2

This structure is based on the most common $2\pi/3$ phase advance constant gradient TW structures and its first, middle and last cells are shown in figure A-2. The variable mesh shown on the figure is for the best simulation of this structure. It is a standard disk-loaded structure with varying aperture size from 4.2 to 3.22 cm in diameter. The aperture size for the first cell is only slightly smaller than the 4.6 cm aperture of the Option 1. However, the aperture size is considerably smaller at the end of the structure. Thus this structure has less beam stay-clear and is less forgiving to transmission and prone to BBU. However it is about 25% more efficient than the Option 1 structure, resulting in a three klystron accelerator scenario with each klystron powering a single 5.15 m structure. Brazing a structure much longer than 3 m has in the past proven to be problematic due to the “book shelving” effect of stacking the accelerator cells in the furnace, however it is possible to divide this structure into two structures to be powered by the same klystron still maintaining its higher efficiency. This would require the addition of two extra couplers. Another drawback for this design is that it requires operating the klystron at peak power and the beam loading compensation, which is achieved by early injection, is not as good as in the baseline design. The energy variation from first to last bunch in this scenario varies from $\pm 3\%$ to $\pm 10\%$ for the high energy cases but due to beam loading, in the low energy case the pulse current is limited to 4.5A to keep the energy spread at below $\pm 13\%$. This is near the maximum the solenoidal magnetic field over the first two accelerating sections can tolerate. The $\pm 10\%$ energy spread for the high energy cases is also difficult for the quadrupole focusing in that region. For the same reasons as explained for the four klystron version of the machine, the first structure powered by the first accelerator klystron would be the only accelerator section in use before the beam is diverted to the low energy experimental station for the user.

The goal for this design option was to save the cost of one klystron while using a conventional traveling wave accelerator section design. If this scenario is chosen by RPI, a more detailed to-build version of this structure in two pieces will need to be designed in the next phase of the project. We will also need to conduct wakefield and beam breakup studies early in the design phase to assure that those factors do not limit the operating range in this scenario and abandon this design if they are an issue. Table A-1 lists the structure parameters, while Table A-2 lists the expected beam parameters and needed klystron power for various modes of operation.

The design phase cost and schedule for this scenario would be very similar to the cost and schedule for the Option 1, eight-structure accelerator, in the main body of this report.

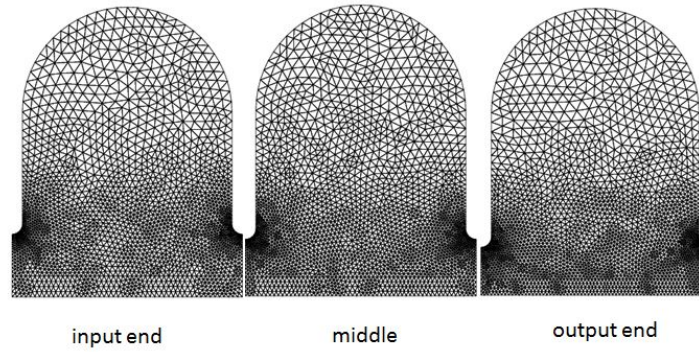


Figure A-1. The first, middle and last cells of the Option 2 constant gradient TW accelerator with gradually reduced aperture from front to end of the structure and variable modeling mesh size to assure an accurate representation of the small curves.

Table A-1 Option 2 relatively low risk and moderately more efficient accelerator structure parameters for the Upgraded RPI 2020 accelerator.

Frequency	1.3 GHz
Structure Type	TW $2\pi/3$
Number of cells	67 (5.15 m)
Aperture $2a$ of first, mid and last cells	4.19, 3.76, 3.21 cm
Attenuation τ	0.478
Ave. Q	23800
Ave. Group velocity V_g/c	0.61%
Ave. Shunt impedance r	53.7 M Ω /m
Filling time T_f	2.79 μ s

Table A-2 Major electron beam parameters and klystron output requirements for the upgraded RPI 2020 accelerator Option 2, utilizing relatively low risk and moderately more efficient accelerator structure parameters.

No. Struc. /No Klys.	Total Active Acc. Length (m)	Beam Inj. Time (ns)	Beam Pulse Length (ns)	Beam Acc. Pulse I (A)	Beam Energy Middle bunch (MeV)	Beam $\Delta E/E$ (%)	Rep Rate (Hz)	Beam Ave. Power (kW)	Klys. Peak Power (MW)	Klys. Ave. power (kW)
3 / 3	15.45	2790	5.4	13	145	± 3.4	700	7.1	14.8	28.9
3 / 3	15.45	1780	250	1.3	136	± 10.4	25	1.1	27	1.4
3 / 3	15.45	1590	1500	0.46	142	± 3	450	43.4	26.9	37.4
1/1	5.15	590	25	4.5*	17.8	± 12.8	800	1.6	26.8	13.2
1/1	5.15	590	25	3.5	18.4	± 9.1	800	1.3	26.8	13.2

* Note that 4.5A is the maximum current that can be accelerated in the low energy scenario and still keep the beam energy spread at $< \pm 15\%$.

Parallel-Fed SW Novel Accelerator Structures for Design Option 3

Very recent R&D at SLAC has resulted in a new concept for standing wave (SW) structures that could be used to design a 16m, three-klystron accelerator system. The accelerator cells in this scenario are each individually fed as shown in Figure A-2



Figure A-2 Novel parallel-fed, very efficient SW accelerator system. Official use only. SLAC Proprietary (Tantawi, 2014)

The parameters for the novel parallel-fed SW L-band structure are listed in Table A-3.

The advantage of this design option is that only three klystrons would be required to power the accelerator of the upgraded RPI 2020 linac, thus saving initial klystron/modulator purchase costs and power costs during operation. In this system the klystrons are not running at their maximum

capacity as in the above 3 klystron scheme, however this being a very novel concept there are higher risks associated with it.

Table A-3 Novel and very efficient accelerator structure parameters for the upgraded RPI 2020 accelerator. Official use only. SLAC Proprietary.

Frequency	1.3 GHz
Structure Type	SW π mode
Number of cells	23 (2.67m)
Aperture 2a of first, mid and last cells	3 cm
Coupling Coefficient β	2.75
Qo	29644
Shunt impedance r	60 M Ω /m

The beam parameters for the various experimental scenarios using this type of structure are shown in Table A-4. One can see that with only three TV-2022D klystrons powering the accelerator structures the required rf power from the klystrons is well within the klystron limits.

Table A-4 Major electron beam parameters and klystron output requirements for the upgraded RPI 2020 accelerator scenario 3, utilizing novel and very efficient accelerator structure parameters. Official use only. SLAC Proprietary.

No. Struct. /No. Klystrons	Total Active Acc. Length (m)	Beam Injection Time (ns)	Beam Pulse Length (ns)	Beam Accel Pulse I (A)	Beam Energy Middle bunch (MeV)	Beam $\Delta E/E$ (%)	Rep Rate (Hz)	Beam Ave. Power (kW)	Klys. Peak Power (MW)	Klys. Ave. power (kW)
6/3	16	1110	5.4	13	148	± 1.3	800	7.0	21.4	19
6/3	16	1110	250	1.07	141	± 5.8	25	1	21.6	0.6
6/3	16	1110	5490	0.27	150	0	200	45	21.4	32.6
2/1	5.3	1110	25	9.8	20	± 14	800	3.9	7.8	7.2
2/1	5.3	1110	25	5.6	20	± 7.8	800	2.2	7.8	7.2

SLAC plans to build and test these structures for other projects in X-band starting in October, 2014 till about May, 2015. However an L-band proof of principal test should be performed and conducted as the first action in the design phase to confirm the design feasibility for use in the RPI linac. These tests would have a major cost impact on the Phase II design program. The necessary prototype design, construction, and high power beam testing will add approximately \$900K to the design phase of the project. Figure A-3 shows a program schedule for the prototype design, construction and testing.

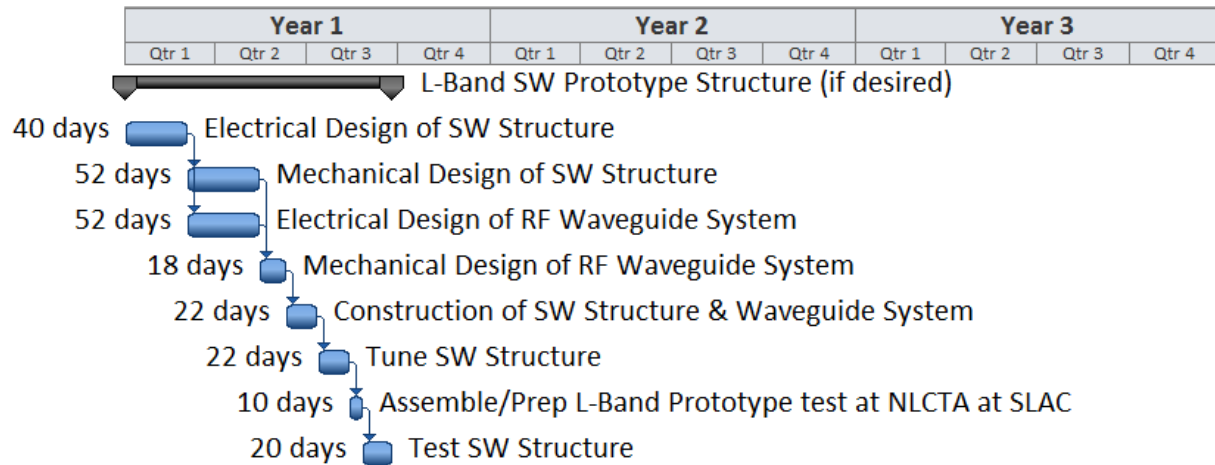


Figure A-3 Program schedule for implementing the parallel-fed SW design.

Appendix B: Bunch stacker

The GELINA neutron spectrometer employs a beam magnetic compression technique called a bunch stacker, which can stack the bunches in a pulse nearly on top of each other, thus shortening the pulse length. A bunch stacker will be necessary for the RPI machine if there becomes a requirement to achieve shorter than 5.4 ns pulse width while maintaining >7 kW average beam power. Note that all accelerator design options in this report are capable of meeting the currently defined beam requirements of the new RPI 2020 accelerator without a bunch stacker.

The beam bunches in the rf linac are equally spaced with a period equal to the rf source wavelength. For the L-Band RPI linac this period is approximately 23 cm and a short train of 5.4 nsec pulses will be ~124.5 cm long. However the individual bunch lengths are much shorter, on the order of 2 cm. There is no charge in the space between the bunches and thus does not contribute to neutron generation, effectively reducing the average current in a pulse. There are methods to reduce the “empty” spaces by compressing the length of the bunch train. These methods are based on the following: The energy of the bunches in the train are slightly reduced from the first to the last bunch (“energy chirp”). This effect can be naturally achieved in a traveling wave accelerator by injecting the beam after the fill time and not compensating for the beam loading effects. The bunch train energy modulation is practically linear if the train pulse width is much shorter than the filling time of the accelerating structure. This linear portion of the energy modulation can be used to compress the train length with a “pulse compressor” beam line between the end of the accelerator and the user experiment. The pulse compressor beam has a magnet system configuration that causes electrons of different energies to take different path lengths. In particular the first higher energy bunch will take a longer path than the last lower energy bunch and since all the electrons are traveling at the same speed (nearly the speed of light), they will nearly converge at the exit of the pulse compressor beam line. The initial length of the bunch train on the target can also be compressed. Given that each electron bunch also has its own energy distribution (because it has a finite size and occupies a finite space on the rf pulse), this distribution may overlap with the distributions of neighboring bunches. The electron energies in the spectrum of a bunch may also be time-correlated depending on where on the rf pulse they have been accelerated. The bunch train (pulse) compression method has been widely implemented at different installations. As an example, a practical application of such an approach has been implemented in the GELINA installation. The GELINA magnet system compresses a 10 nsec bunch train with S-Band bunch separation down to 1 nsec.

One example of a pulse stacking concept that could be implemented in the RPI facility is shown in Figure B-1. This concept uses a long horizontal path length with two bend magnets to stack the pulse. The disadvantage of this approach is the long length of the beam line. An alternative bunch stacker layout is shown in Figure B-2. In this layout a scaled version of the GELINA magnet compression scheme is utilized which yields a more compact bunch stacker. The horizontal length of the installation would be only 3 ft. However the magnet installation would require excavation of the floor in order to maintain the existing vertical height. (5 ft) of the linac beam line

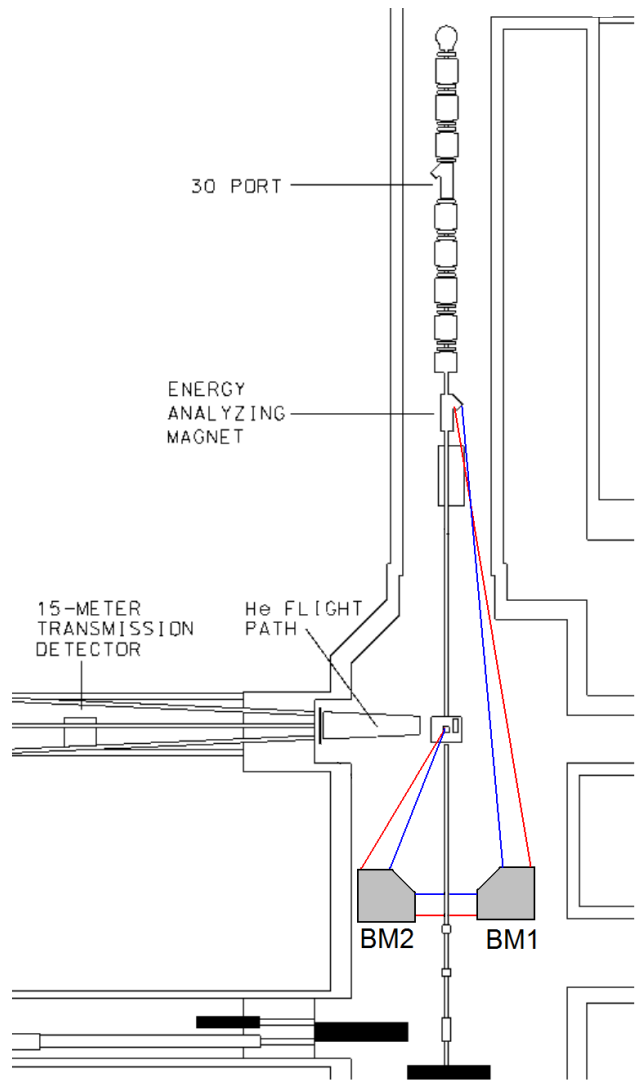


Figure B-1. Implementation of a bunch stacker beamline in the RPI bunker. The layout employs two bending magnets BM1 and BM2. Red and blue traces are the trajectories for the “high” and “low” beam energies

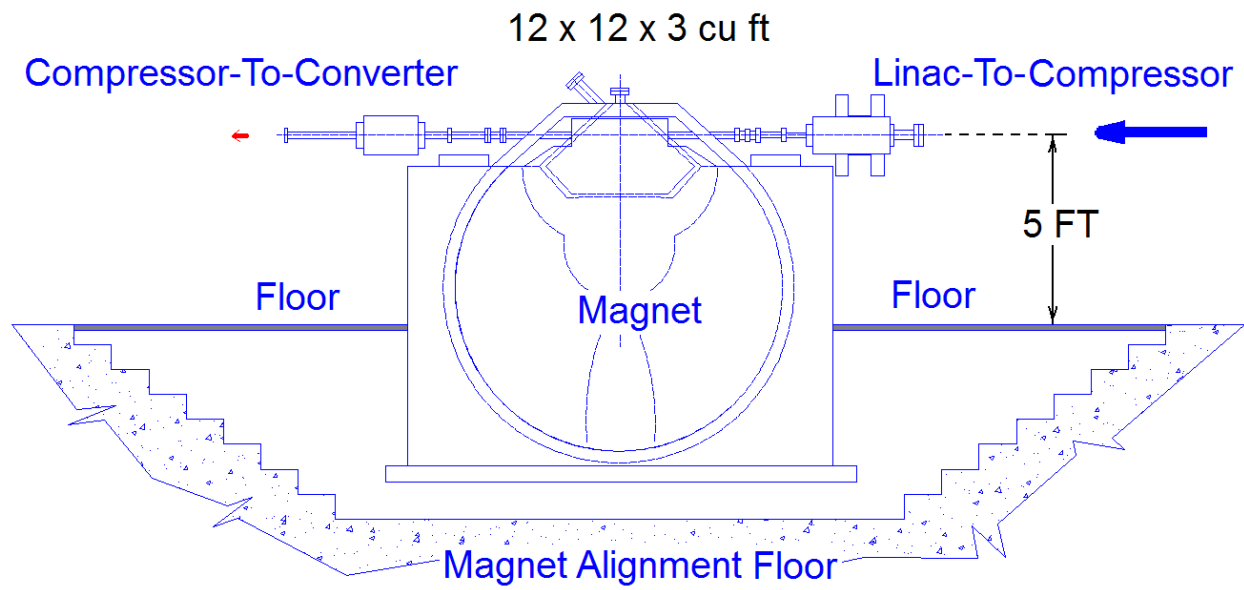


Figure B-2. Implementation of a GELINA type magnet system in the RPI bunker.

Appendix C: RF Pulse Compression

The SLAC Energy Development (SLED) system was invented in 1976 in order to nearly double the SLAC linac energy without changing its accelerator configuration or the number of klystrons needed to feed them [9]. The method relies upon two high Q resonators storing energy from an rf source for a relatively long time interval (typically 3-5 μsec). Triggered by a reversal in rf phase, this stored energy is then released during a much shorter interval equal to the filling time of the accelerating structure plus the beam pulse length. A SLED energy storage network at a typical klystron station at SLAC is shown in Figure C-1.

Figure C-2 shows the SLED waveform progression, The shape of the output rf power pulse is, however, a sharply decaying exponential which causes a decrease in effective power gain. The other sources of loss are reflections during charging, energy left in the cavities at the end of the pulse, and energy loss inside the cavities.

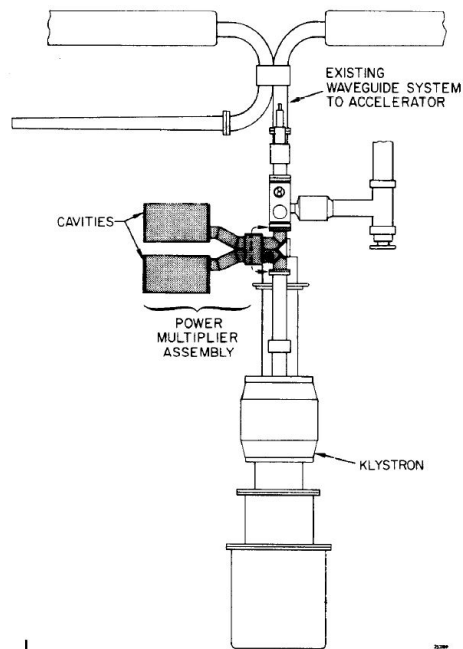


Figure C-1. SLED Energy storage network at a typical klystron station at SLAC.

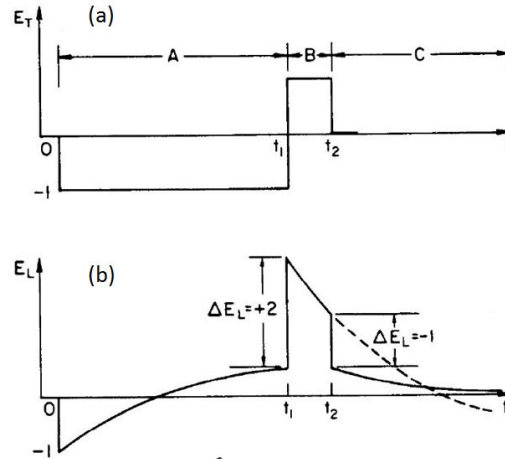


Figure C-2. SLED waveforms (a) the input waveform from the klystron instantaneous phase reversal at $t=t_1$, (b) the SLED output waveform.

The SLAC SLED can compress a ~ 60 MW, $3.5 \mu\text{s}$ klystron output pulse into a 160 MW, $0.82 \mu\text{sec}$ accelerator input pulse. A peak power gain on the order of three and a compression efficiency on the order of 60% is typically attained. However the upgraded RPI 2020 accelerator operation has several operational scenarios with $>3.2 \mu\text{sec}$ rf pulse length, and the entire stored energy of the full klystron pulse. The Thales TV-2022D klystron with a $7 \mu\text{s}$ pulse length has neither enough pulse length nor enough stored energy to make use of a SLED system for the various beam operation scenarios needed at RPI.

Appendix D : SLAC Surplus

Currently SLAC is planning to dismantle the first 1/3 of its 3 km linac to build the Linac Coherent Light Source II, which unlike its predecessor in the final third of the 3 km linac will be a cryogenic machine. Many components, such as magnets, diagnostics, and valves, will become available for the cost of removing them carefully from the accelerator tunnel. These components can be offered to RPI, and SLAC personnel have the best knowledge of the characteristics of these components (calibration curves, power requirements, and so on) and how to best apply them to the new RPI machine.

References

1. Swanson, W. P., “Calculation of Neutron Yields Released by Electrons Incident on Selected Materials”, Stanford Linear Accelerator Center, Stanford, California, SLAC-PUB-2042, 1977
2. RPI staff, “Linac 2020 Upgrade – Specifications of Operating Modes, RPI/SLAC communication”, April 2, 2014
3. Wang J. W., Adolphsen, C., Bharadwaj V., Bowden G., Jongewaard E., Li Z., Miller R. H., Sheppard J. C., “Positron Injector Accelerator and RF System for the ILC, SLAC National Accelerator Laboratory”, Stanford, California, SLAC-PUB-12412, March 2007
4. Koontz, R. F., “CID Thermionic Gun System”, Proceedings of Linac81, Santa Fe, New Mexico, 1981.
5. Herrmannsfeldt, W. B., “EGUN- An Electron Optics and Gun Design Program”, SLAC PUB-331, Stanford Linear Accelerator Center, Stanford, California, 1988 .
6. Yeremian A.D., “Boeing 120 MeV RF Linac Injector and Accelerator Performance Comparison with PARMELA”, IEEE Proceedings of the Particle Accelerator Conference 1989, Chicago Illinois, March 1989
7. Panofsky W. K. H., “The Use of a Long Coaxial Ion Chamber Along the Accelerator,” SLAC TN-73-57 Stanford Linear Accelerator Center, Stanford, California, 1963
8. Rolfe J., Gearhart R., Jacobsen R., Jenkins T., McCormick D., Nelson R., Reagan D., Ross M.C., “Long Ion Chamber Systems for the SLC”, SLAC PUB 4925, Stanford Linear Accelerator Center, Stanford, California, March, 1989.
9. Farkus Z. D., “SLED: A Method of Doubling SLAC’s Energy”, Proceedings of the 9th International Conference on High Energy Accelerators, p 576, May 1976.